POLITECNICO DI TORINO

Master's Degree Thesis in Biomedical Engineering

Master's Degree Thesis

Cardiac and Respiratory analysis from photoplethysmographic (PPG) signal for stress and mental workload assessment

Supervisors

Prof. Danilo DEMARCHI

Ph.D. Irene BURAIOLI

Ph.D. St. Gabriele LUZZANI

Candidate

Antonello SEMERARO

March 2025

Summary

The World Health Organization (WHO) has included burnout in the International Classification of Diseases. Consequently, real-time monitoring of an individual's stress levels and mental load while performing a task is crucial to assess whether the person is actually able to complete the assigned task. The analysis of physiological signals is the best strategy for real-time monitoring of mental workload, which have distinctive characteristics related to the individual's physiological state. In particular, the cardiac and respiratory signals have characteristic features, such as heart rate (HR), heart rate variability (HRV), and respiratory rate (RR), that are highly dependent on mental workload levels. However, the necessity of acquiring each signal with a dedicated system gives rise to issues concerning the footprint, which hinders the task to be performed. In order to overcome these limitations, recent wearable devices can be utilised for the purpose of acquiring the photoplethysmographic (PPG) signal from which the extraction of both cardiac and respiratory characteristics is possible. This development has the potential to significantly reduce the user's bulk associated with conventional acquisition systems. The aim of this study is to extract the respiratory signal from the PPG signal. This is achieved by focusing on the detection of the respiratory frequency and on the morphology of the signal itself. A novel algorithm on the MATLAB® platform that employs a diversified strategy for the extraction of respiratory signal, depending on the quality of the signal, has been developed. The first step in extracting the respiratory signal involves implementating a low-pass filter with a cutoff frequency of 0,65Hz. After the filtering phase, a statistical analysis to verify the cleanliness of the signal is conducted. In the event that the filtered signal is clear, the algorithm employs a spectral analysis method in order to identify the respiratory frequency. Conversely, when noise is present, the Empirical Mode Decomposition (EMD) for signal decomposition is applied. This solution ensures enhanced computational efficiency and is particularly well-suited to a real-time context, offering a sophisticated and expeditious methodology for monitoring the respiratory signal. The efficacy of the algorithm was tested on the Capnobase data set, consisting of 42 physiological signals including respiration and PPG, acquired at rest for 8 minutes. The results are compared with the respiration

rate values obtained on the same dataset using the Smart Fusion algorithm. The comparison demonstrated that the former led to superior results, especially for very noisy signals on which the latter was unable to perform. The validation of the algorithm was achieved by creating an experimental data set using the BiosignalplusX device, which is capable of acquiring the ECG, respiratory signal, and PPG signal simultaneously. Patients firstly underwent a resting phase and subsequently an N-Back test, the purpose of which was to stimulate cognitive function. The algorithm demonstrated remarkable efficacy in identifying respiratory and heart rate by directly comparing the extracted data with the acquired references. In the assessment of mental load, the extracted feature distribution were compared with the results of subjective questionnaires, which investigated the perception of cognitive effort during the test.

Table of Contents

Acronyms

AI
Artificial Intelligence

BP
Blood Pressure

DC
Direct Current

DPF
Differential Pathlength Factor

ECG
Electrocardiogram

EEG
Electroencephalography

EOG
Electrooculography

EMD
Empirical Mode Decomposition

ERP
Event-Related Potentials

fMRI
Functional Magnetic Resonance Imaging

fNIRS

Functional Near-Infrared Spectroscopy

GAD

General Adaptation Syndrome

HR

Heart Rate

HRV

Heart Rate Variability

IIR

Infinite Impulse Response

LED

Light-Emitting Diode

LMS

Least Mean Squares

MWL

Mental Workload

NASA-TLX

National Aeronautics and Space Administration Task Load Index

N-F

Nasal-Forehead (temperature measurement)

PPG

Photoplethysmographic

PFC

Prefrontal Cortex

RSA

Respiratory Sinus Arrhythmia

RR

Respiratory Rate

SWAT

Subjective Workload Assessment Technique

WHO

World Health Organization

Chapter 1

Introduction

In the modern society, people often face challenging situations, whether in their work or everyday life. These challenges can lead to increased stress and mental exhaustion. According to the World Health Organization (WHO), mental stress has become a global epidemic in the 21st century [1].

The situation has worsened since the Covid-19 pandemic. One of the main causes of increased stress levels is the social isolation caused by thepandemic, which has limited people's ability to work and actively participate in their communities. The intensification of these factors has led to a significant increase in burnout. Research shows that 25% of workers have health problems due to psychological stress related to work [2]. Burnout is a state of physical, emotional and mental exhaustion resulting from prolonged and excessive stress, usually related to a work environment or tasks that require intense and continuous commitment. It occurs when an individual faces persistent stress over an extended duration without sufficient time for proper recovery [3]

The WHO acknowledges burnout as a condition associated with inadequately managed chronic stress at work and has included it in the International Classification of Diseases. This state of exhaustion can reduce a person's ability to perform their tasks or daily responsibilities efficiently [4].

For this reason, monitoring of stress and mental workload parameters is becoming increasingly important. Over the years, various methods to assess stress levels have been proposed which can be divided into subjective assessment, behavioral assessment, and physiological assessment. However, the first two methods provide a subjective evaluation of the parameters, relying on questionnaires or direct observation of the patient's behavior. These methods do not allow for real-time monitoring, for instance, of individuals engaged in precision-demanding tasks. Consequently, efforts are focused on improving physiological assessment. Physiological assessments analyze physiological signals. The most commonly studied are heart activity, skin activity, eye activity, brain activity, respiration, body temperature,

muscle activation and voice patterns. It is evident that each of these corresponds to a signal from which a specific feature can be derived. These features are influenced by stress and cognitive load; therefore, they can be studied in order to monitor stress and mental workload parameters. Obviously, simultaneous monitoring of all these signals would lead to a much more accurate and reliable analysis of cognitive workload status. However, it is important to highlight that capturing each of these signals necessitates a specialized detection system that interacts with the patient through carefully positioned electrodes. This would inevitably result in evident bulk issues, consequently leading to constrained mobility and a state of discomfort, especially in situations where the application is meant for individuals performing specific tasks or work-related activities. A solution can be obtained by extracting as much information as possible from a single biological signal. The redundant sensors can then be removed. The primary illustration of this phenomenon is the observed correlation between respiratory and cardiac activity. Respiration has long been shown to correlate with certain aspects of the electrocardiogram,such as respiratory sinus arrhythmia (RSA). RSA is a natural and physiological variation in heart rate that occurs in response to respiratory cycles. For example, during inhalation the heart rate tends to increase (tachycardia), while during exhalation it tends to decrease (bradycardia). This phenomenon is known as respiratory bow or respiratory synchrony. This implies that the heartbeat and breathing are naturally synchronised [5]. To exploit the full potential of this system, it is necessary to look for a signal with the most convenient sensor system. One of the most studied signals in this sense, due to its ease of acquisition, is the photoplethysmographic (PPG) signal. Traditional photoplethysmographs that measure blood volume saturation are usually worn on the finger. However, in some cases it is placed on the head, i.e. the ear, nasal septum and forehead [2]. In recent years, advancements in technology have led to the development of wereable devices capable of reliably acquiring the photoplethysmographic signal. The PPG sensor measures changes in blood volume under the skin using light emitted by the sensor and reflected by the blood vessels. As the heart beats, the amount of blood flowing through the vessels changes, causing the amount of reflected light to change [6]. The photoplethysmography (PPG) sensor is capable of detecting changes in light intensity and translating them into a signal. Consequently, the most direct and immediate analysis is that of cardiac feature extraction. However, over the years, many studies have focused on understanding the influence of respiration on the PPG signal by trying to identify the correct respiratory rate.

The objective of this thesis is to examine the feasibility of deriving the respiratory signal from the photoplethysmographic (PPG) signal. This effort involves not only the identification of the correct respiratory frequency, but also the emphasis on the appropriate waveform to ensure the accurate extraction of respiratory features. It is important to note that a significant number of respiratory features depending

on the positioning of peaks and valleys. Observations concerning the influence of stress and cognitive load on features such as the time and volume of inhalation and breathing are made using the position of signal peaks and valleys. Consequently, enhancing this aspect would result in more precise and reliable analyses. Once validated, the use of one of the new sensors integrated into wearable devices to extract cardiac and respiratory data could becomes feasible, thus greatly improving the comfort of the monitored individual. When thinking about wearable devices, people often associate them with gadgets such as smartwatches.; however, recent advancements in research have led to the development of other devices, such as the Oura Ring [7] in Figure 1.1 and On Ear [8] in Figure 1.2.

Figure 1.1: Image of a commercial smart ring, the Oura ring, showing the LEDs used to emit light and detect the PPG signal

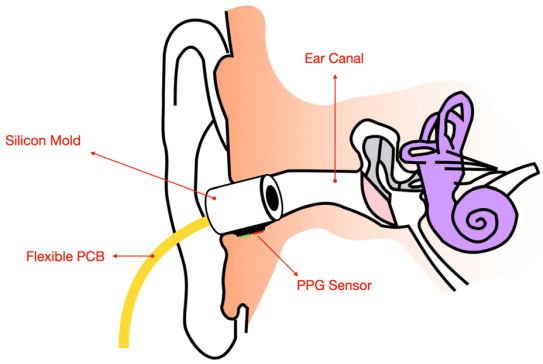

Figure 1.2: Representation of the custom-built PPG ear tip inside the ear canal

These innovations, characterized by enhanced adhesion to the body region or incorporation of accelerometers and gyroscopes, have enabled a substantial reduction in movement artifacts that are prevalent in photoplethysmographic

(PPG) signals, thus broadening their practical applications. Consequently, the study and analysis of the PPG signal are currently more important than ever, given the potential of the signal itself.

Chapter 2

Background

2.1 Stress

The word 'stress' originates from the latin term 'strictus', meaning 'tight'. Stress is described as a mental state of preoccupation triggered by a challenging circumstance or a gap between environmental demands and personal resources. The environmental phenomena that cause an individual's state of stress are designated stressors. The term 'stressor' is employed to denote events, causes and harmful agents that have the potential to induce a General Adaptation Syndrome (GAD). These stressors can be categorised into four distinct classifications: physical, metabolic, psychological, and psychosocial stressors. The response to stressors is entirely subjective and varies from individual to individual [9]. As a result, it is not guaranteed that individuals with varying personal backgrounds, experiences, and psychophysical conditions will experience the same degree of mental distress in response to a particular situation. Hans Selye, a pioneering figure in the field of stress research, proposed a two-category system to categorise stress: eustress, also known as positive stress, and distress, also known as negative stress. Eustress is essential for achieving goals, as it facilitates the optimal utilisation of energy to accomplish the objective. This is facilitated by the body's ability to counter external stimuli with effective mechanisms that enable adaptation to the prevailing circumstances [10]. Distress gradually accumulates within an individual, activating compensatory hormonal responses. Over time, this can lead to a breakdown of psychophysical defenses, either preventing the person from deploying protective mechanisms against the stressor or causing the activation of ineffective coping strategies [10]. Hans Selye originated a model of GAD which consists of three phases as shown in Figure 2.1:

1. **Alarm**: The first phase is known as the alarm phase. During this phase, the individual is in contact with a stressor, which causes physiological dysfunction.

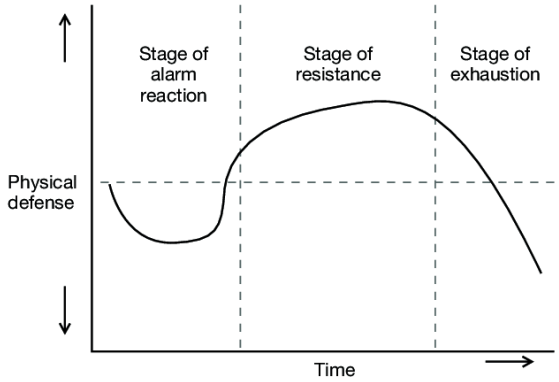

Figure 2.1: General adaption syndrome. The following is a description of the physical response according to the stressful phase in which the individual is currently situated.

In response, the neurovegetative system triggers a counter-shock reaction. As a result, the body begins to generate energy to adapt to the challenge. More significant physiological changes occur during this phase, caused primarily by the activation of the sympathetic nervous system, which mobilizes additional resources to effectively manage the stressor.

2. **Resistance**: during the resistance phase, physiological changes continue to allow the individual to adapt to stressors. However, if these external stimuli are removed while the sympathetic nervous system is active, prolonged stimulation can have detrimental effects on the body. Prolonged physiological tension can contribute to the development of stress-related diseases

3. **Exhaustion**: If resistance to stressors fails to produce a favorable outcome, one enters the exhaustion phase. The effects accumulated so far lead to functional impairment.

2.1.1 Work related stress

Work-related stress is a physiological and emotional response that arises when job demands exceed the capabilities of the individual. In the domain of theoretical models of work stress, a seminal contribution was made by Cooper and Marshall (1978) [11] who developed a model, subsequently refined in 1988 by Sutherland and Cooper [12], which categorizes the sources of work stress into [13]:

- **Sources intrinsic to the 'job':** Physical and environmental factors that can negatively impact workers' concentration, performance, and efficiency.

Noise, inadequate or overly bright lighting, and poor environmental hygiene are included.

- **Organization:** A distinction is made between role ambiguity, which refers to a lack of clarity regarding job tasks, and role conflict, which arises not from excessive demands but from mutually incompatible expectations. This concept can be further divided into four categories: role-person conflict, where the individual prefers tasks different from those assigned; role overload, where the workload exceeds the individual's capacity; intramandatory conflict, where the available staff is insufficient to complete the task; and inter-mandatory conflict, where a task is acceptable to some but undesirable to others.

- **Career development:** It can become a major source of stress for people with strong aspirations to attain a high socioeconomic status, especially when these aspirations remain unfulfilled.

- **Work relationships:** The following challenges may arise in relation to colleagues, superiors, or subordinates. Four distinct relational stressors have been identified: position inconsistency, where the role an individual occupies differs from the one they desire; social density, referring to inadequate living or working space; abrasive personality, where individuals exhibit insensitive behavior towards others' emotions, creating stress in relationships; and leadership style, which refers to how a superior interacts with subordinates. For example, an authoritarian style may lead to less employee engagement, fostering apathy or tension, while a democratic style encourages greater involvement and motivation among workers.

- **Organizational structure and climate:** The way an individual perceives the company climate and how they evaluate the demands made by superiors greatly influences their ability to develop socialization and work motivation.

Monitoring work-related stress has been shown to have a significant impact on an individual's health and job performance. It is critical to recognize that high levels of work-related stress can lead to burnout.

2.2 Mental Workload

2.2.1 Introduction

Despite various attempts over the years, a consensus on the definition of mental workload has yet to be reached. However, it is widely accepted that cognitive load, and therefore mental effort, is acknowledged and valued to the same degree

as physical effort, as long as it is measurable and real [14]. Mental workload can be defined as the interaction between the operator and the task assigned to them, in the presence of repetitive operations [15]. Mental workload refers to the cognitive demand that a task or group of tasks places on the limited processing capacity of the human brain, similar to how physical exertion uses the body's resources. It is important to emphasize that the term 'limited' in this context does not suggest infinite capacity [16]. The human mind, similar to computers, is subject to structural limitations that delineate its capacity. The vast area can be represented by the operator workload into three subgroups [15]: Input workload, Operator Effort, Performance (or result of the work performed) as in Figure 2.2. The feedback given by the operator after the tasks have been performed is also important.

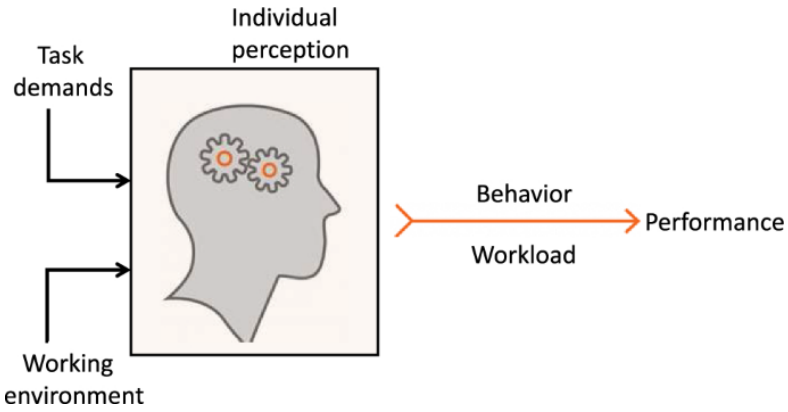

Figure 2.2: The following schematic representation illustrates the mental workload of an operator

The input workload consists of external events that are not directly controllable by the operator. The major sources of input load can be separated into three main classes:

- **Environmental:** These include noise, vibration, and temperature, along with various stimuli from the external environment that are difficult to manage or control
- **Induced by design or situation:** This encompasses the characteristics of the displays and devices used, the layout of the work area, and the dynamics of the machinery. It refers to everything that forms the physical "framework" upon which tasks are built
- **Procedural:** This involves the briefing and instructions, the sequence of tasks to be completed and the expected duration. The operator's effort is

determined by several factors, including the input load and the performance demands of the task assigned

The concept of effort pertains to the mental and emotional energy expended by an operator in order to engage in a given activity. Effort functions not only as an indicator of performance, but also as a metric that quantifies the intensity and nature of mental and emotional endeavor. This is contingent upon a multitude of complex and interrelated factors inherent within the individual. In particular, a distinction is made between:

- **Stable factors:** These characteristics remain relatively stable over time and play a fundamental role to defining an individual. They include psychophysical attributes (e.g., health status and cognitive capacities), personal background (such as education and past experiences), and personality traits (e.g., resilience or predisposition to stress)
- **Fluctuating factors:** These variables are subject to change over time and exert a more dynamic influence on effort. They include prior experience accumulated in similar contexts, momentary motivation (the extent to which an individual is engaged or driven to complete a task) and attentional focus (the degree of concentration directed toward the task at hand)

While an operator may achieve a comparable level of performance in disparate situations (e.g. in systems designed differently but with analogous purposes), it is imperative to consider the effort expended to attain that result [17]. This is due to the fact that the end result alone does not provide a complete understanding of the extent of mental or physical effort expended by the individual. In essence, the effort expended can vary significantly between tasks that yield the same outcome, underscoring the necessity for quantifiable metrics in comparative analyses, particularly in contexts involving diverse physical and mental workload demands. Performance is generally classified as the set of useful data generated as an output of the work performed by the operator.

2.2.2 Effective and ineffective workload

Cognitive load can be classified as either effective or ineffective. Effective load refers to the minimal workload necessary to complete a task and represents the portion of effort that directly contributes to task accomplishment. Conversely, ineffective load encompasses the extraneous effort that does not facilitate task completion and could be reduced through learning and training. From the perspective of task execution strategies, effective load is characterized by swift and accurate performance, whereas ineffective load is associated with errors and reduced precision [18]. The effective workload requires fewer cognitive resources as it is linked to

efficiency. In contrast, the ineffective portion of mental workload demands greater cognitive resources to manage each stage of information processing. Recognizing mental workload is a crucial factor in the design and development of occupational tasks [19]. The interaction between the operator and the assigned task serves as a critical metric, providing insight into areas where task demands can be increased without compromising performance and identifying situations where such an adjustment could negatively affect human efficiency. It has been demonstrated that an increase in task difficulty, or a decrease in the time allocated for completion, results in an increase in workload. Task demands must be carefully calibrated to prevent both overload and underload, thereby promoting safety, well-being, comfort, and sustained productivity. The latter aspect is of particular significance in the context of developing valuable human resources. It is evident that extended periods of elevated cognitive load can result in suboptimal processes, diminished performance, and even potential repercussions on the worker's mental well-being [20]. It can thus be concluded that cognitive load can be adjusted either by increasing the available cognitive resources of the individual or by decreasing task demands. Measuring mental workload is essential for optimizing these processes.

2.2.3 Burnout

The condition characterized by prolonged chronic stress and excessive workload, leading to a state of exhaustion, is known as burnout. It is characterized by physical, emotional, and mental exhaustion resulting from prolonged and excessive stress, most commonly in work-related environments [21]. This condition is characterized by three main symptoms: emotional exhaustion, depersonalization, and a reduced sense of personal accomplishment [22]. The World Health Organization (WHO) has officially recognized and classified burnout as a syndrome within the framework of occupational health. According to the WHO, burnout is defined as "a syndrome conceptualized as a consequence of chronic stress in the workplace that has not been successfully managed." This indicates that work-related stress is regarded as a condition that can impact an individual's health and well-being. While the WHO has provided diagnostic guidelines for burnout, it has not established specific treatment or cure protocols. The symptoms of burnout are as follows (Figure 2.3):

- **State of exhaustion**,both mental and physical, which may be accompanied by symptoms of anxiety, depression, or other psychological disorders. These symptoms may also be accompanied by a range of physical disorders, including headaches, gastrointestinal disorders, sleep disturbances, chronic fatigue, and an increased vulnerability to stress-related physical illnesses, such as cardiovascular or immune system disorders.
- **Increased mental distance from one's work**, negativity and cynicism

related to one's occupation/role.

- **Reduced professional effectiveness** consisting in lack of concentration and motivation can adversely can negatively impact work performance by leading to errors. Additionally, decreased mental and physical energy may result in a general decline in the quality of work, with less attention to detail and diminished overall output.

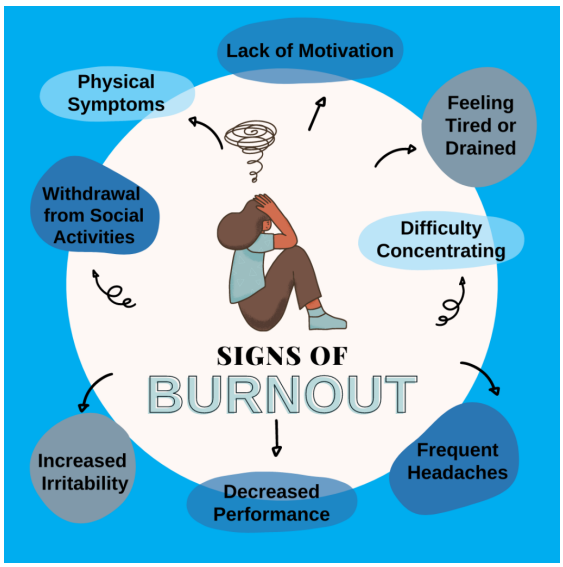

Figure 2.3: Burnout symptoms that an individual may experience

2.2.4 Why measure mental workload?

The concept of mental workload refers to the cognitive demands an individual must manage while performing a task or a series of tasks. This concept primarily originates from the field of performance measurement, which focuses on assessing an individual's ability to complete specific tasks. The core assumption of this concept is that humans function as 'one-channel' systems, implying a limited capacity to process information or handle tasks simultaneously. This theoretical approach has significantly influenced workload research, leading to the belief that an individual's cognitive capacity is constrained during a single task, potentially resulting in reduced performance. However, this 'single-channel' model is considered insufficient, as it overlooks the complexity and variability inherent in tasks. For example, measures of effort in a single task may not fully capture the workload, as different tasks have unique characteristics that affect the individual in distinct ways. Furthermore, there is an absence of universal metrics with which to compare

workload across tasks of a significantly different nature. As a result, research is increasingly focusing on understanding cognitive workload in a more detailed way, recognizing that humans aren't just one-task beings. Instead, people are capable to manage multiple tasks at the same time, as long as the tasks fit together and the conditions are right. For instance, certain activities may be executed in parallel without inducing cognitive overload, while others might necessitate exclusive attention, .

The measurement of mental workload and, in a related manner, stress, especially in critical work contexts, has become critical for several reasons:

- **Performance optimisation:** Determining whether the individual being analyzed is overloaded can offer valuable insights into their performance. Overload typically results in a decline in work performance, significantly increasing the likelihood of errors, while an excessively low workload may suggest that the task is insufficiently stimulating to fully engage the individual and harness their full potential(Figure 2.4)

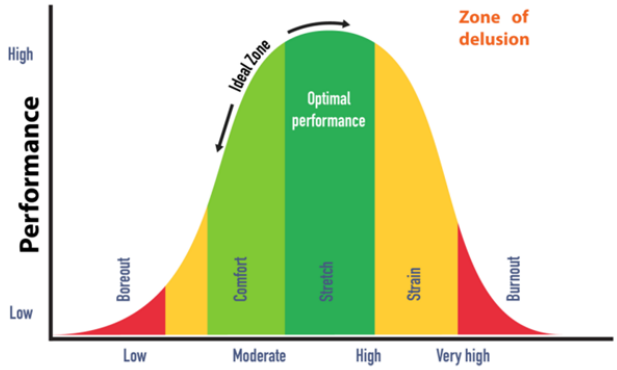

Figure 2.4: Performance trend as a function of the pressure the operator is subjected to

- **Burnout prevention:** keeping cognitive load and stress levels under control is important to avoid burnout with the consequences in terms of physical and mental exhaustion that it entails
- **Safety:** in critical work environments, making mistakes due to mental overload can lead to catastrophic consequences. Preventing this condition would increase the safety of workers and the environment
- **Designing the work environment:** understanding how a task is perceived at the level of the mental resources involved is useful for designing work

environments that are more efficient and suited to human capabilities. One of the initial applications of mental workload research was in the design of user interfaces, with the goal of simplifying tasks and making them more understandable and user-friendly

- **Effectiveness in strategic decisions:** For human resources managers, measuring workload provides valuable insights for making informed decisions regarding the planning, delegation, and monitoring of activities. With precise data, more effective strategies can be implemented to enhance overall efficiency and achieve business goals

Finally, although it is important to predict workload, it is equally crucial to develop measurement methods that do not interfere with the performance of the tasks themselves. This is to enable the effective monitoring of workload without adversely affecting the individual's performance or experience during the task.

2.2.5 Methods for measuring MWL

In measuring workload, a fundamental distinction is made between experimental (laboratory) and operational (real-world) environments. In experimental environments, measurement are often more comprehensive and offer different methods for to analyze empirical conditions and collect detailed data. The application of these techniques in operational settings presents challenges, including concerns about ecological validity (i.e., how well the laboratory environment reflects real-world conditions) and the influence of individual differences. In contrast , measuring workload in real-world situations is further complicated by complexity of the operational context, variability in individual differences of operators, and the difficulty of accounting for how changes in strategies may impact both performance and measurement results.[23].

A set of criteria for selecting or developing suitable techniques for measuring mental workload [23] are reported:

1. **Sensitivity to changes in the task:** the measurement method must be sensitive to changes in the difficulty of the task or in the demand for resources, being able to distinguish between significant changes in the workload

2. **Diagnosis of sources of variation:** the method must be able to identify the source of variations in workload, such as the type of task or resources required.

3. **Non-invasive:** the measurement technique must not interfere with the operator's activity, either mentally or physically, and must not itself become a source of mental workload

4. **Acceptability by practitioners:** It must be a technique that subjects easily accept, without being too intrusive.

5. **Simplicity of tools:** The technique should require a minimum of equipment so that it does not adversely affect performance

Additionally, other criteria have been suggested, such as the ability to respond quickly to fluctuations in workload and the capacity to demonstrate reliability and consistency over time. Furthermore, it is crucial that the technique is specifically sensitive to changes in mental workload, while remaining highly resistant to external factors, such as emotional stress or unrelated physical stresses, that may not be relevant to the measurement. In general, workload measurement techniques must be designed to meet these criteria so that they can be successfully applied in operational environments, where conditions are less controllable than in experimental settings. The accuracy of measurement is contingent on the ability to consider individual differences between operators, adapting techniques to adequately reflect the different capabilities and resources available to each individual.

It is generally accepted that mental workload can be estimated using three main types of measures: self-report measures, primary performance measures, and physiological measures.

2.2.6 Self-report measures

Subjective measures collect direct feedback from workers about the mental effort they experience while performing certain tasks. These tools are considered non-intrusive and easy to use, and they are supported by strong theoretical foundations due to their ability to offer valuable insights into a worker's workload and cognitive demands. In numerous self-report-based measurements, subjects are invited to respond to a questionnaire before and/or after a task [24]. This strategy aims to identify possible performance biases that a worker might exhibit due to their mental state before the task. The majority of subjective measures are administered after the task has been completed and can be further subdivided into:

- **One-dimensional**
- **Hierarchical**
- **Multidimensional**

Unidimensional self-reports usually provide a single overall value, expressed through a numerical or categorical scale with varying ranges, either in written or verbal form. While this approach is unquestionably straightforward in terms of data acquisition due to its non-invasive nature, it has been argued by some that these assessments

lack a structured framework and provide limited or poor information for diagnostic purposes [25]. One-dimensional scales are predicated on the conceptualisation of workload as a continuum, with the Rating Scale Mental Effort [26] and the Instantaneous Self-Assessment Workload [27] being notable exemplars.

In hierarchical evaluations, operators make a series of decisions, with each response leading to a new choice or a final numerical evaluation [25]. Examples of hierarchical ratings include the Modified Cooper Harper Scale [28] and the Bedford Scale [29].

Multidimensional assessments are based on the idea that evaluating individual components offers greater reliability for practitioners than a single, overall assessment. Unlike unidimensional assessments, these measures provide diagnostic insights into specific sources of workload, along with an overall summary. An example of a multidimensional assessment is the NASA-TLX, [30], the Workload Profile [31] and the Subjective Workload Assessment Technique (SWAT) [32].

The NASA-TLX is the most commonly used tool for assessing mental workload, followed by the SWAT, the Rating Scale Mental Effort, and the Workload Profile. These multidimensional scales have been applied across a wide range of disciplines, sectors, and fields of application, largely due to their ease of use and the strong recognition they have gained within this area of research. [33]. Multidimensional assessments are widely regarded as having high sensitivity and diagnostic capacity, with low levels of intrusiveness and convergent validity [32]. However, it is important to note that some issues have been identified with these scales. For example, the SWAT scale, which is based on the assumption of joint analysis, deviates from this assumption in several cases [34]

National Aeronautics And Space Administration – Task Load Index (NASA-TLX) The NASA-TLX is a subjective workload assessment instrument. Its origins lie in the US civil and military aerospace field (where it was developed by NASA), yet it has found applications in numerous other domains, including nuclear, automotive and manufacturing. It is used as a benchmark for evaluating and assessing new MWL measures. On the technical side, NASA-TLX utilizes a multidimensional scale to measure an operator's performance while completing a task. The scale consists of six sub-scales, which are as follows:

1. **Mental demand:** measures whether the perceptual activity is easy or complex

2. **Physical demand:** measures whether the physical activity performed during the task is exhausting or relaxing

3. **Time demand:** measures the amount of pressure felt by the operator in relation to the pace of execution required by the task

4. **Effort:** measures the difficulty of the work done in order to complete the task

5. **Performance:** measures the subject's satisfaction with the execution of the task

6. **Frustration levels:** measures the subject's mood in performing the task

There are seven steps for implementing the NASA-TLX, as outlined in Figure Figure 2.5:

1. Definition of the activity subject to analysis.

2. Hierarchical Task Analysis (HTA) to define and better understand the characteristic steps of each task.

3. Participants are selected in such a way as to meet the needs of the experimental design.

4. Briefing to explain the NASA-TLX and the purpose of the study the participants are taking part in.

5. Task execution.

6. Implementation of the NASA-TLX itself. Fifteen pairwise combinations are shown to the participants, who are asked to identify which ones, in their opinion, had the most significant impact on their cognitive workload during task performance. Following this, the evaluation questionnaire is administered, incorporating the six steps previously outlined.

7. The final step involves processing and analyzing the results obtained.

The most prevalent modification to the NASA-TLX is the elimination of the section pertaining to pairwise comparisons, which results in what is termed the RAW NASA-TLX.

Workload profile The workload profile is a multidimensional subjective measurement tool based on the multiple resources model proposed by Wickens in 1987. This method uses eight dimensions to gather data on the cognitive demands of tasks, including perceptual/central processing, selective response execution, spatial, visual, verbal, and auditory processing, as well as manual and discursive outputs. The method provides an overall rating for each task, along with individual ratings for each workload dimension. These multidimensional ratings are thought to offer a comprehensive understanding of the level of MWL, helping to categorize tasks based on their relative demand for effort. Below are the steps that make up the test, also shown in the image Figure 2.6:

1. Specify the task or scenario under analysis.

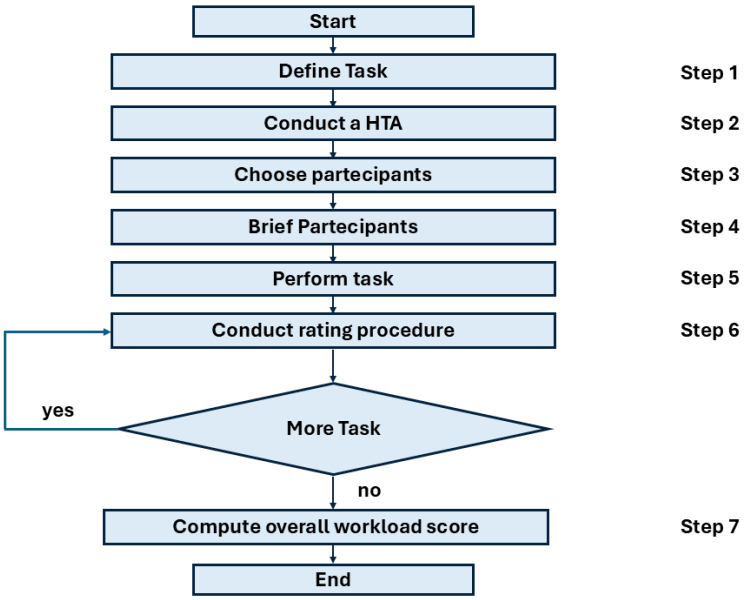

Figure 2.5: Workflow representing the various steps in the NASA-TLX test

2. Perform Hierarchical Task Analysis (HTA) to better understand the process that characterizes the task.

3. Creation of a pro forma workload, which consists of a list of task activities in random order, displayed in a column. The other columns of the table to be created should contain the different dimensions of the MRT, namely:

   (a) Processing state (perceptual/central vs. response)

   (b) Input modality (visual vs. auditory)

   (c) Output modality (manual vs. vocal)

   (d) Processing code (verbal vs. spatial)

Selection of participants.

Participants attend a briefing, during which the method and purpose of the experiment are explained. It is recommended that participants undergo a workshop on MWL, its recognition, the theory of multiple resources, and the dimensions that define the workload profile prior to the study, to enhance their understanding of the process. This preparation is crucial, as the actions and conclusions of the operators serve as the foundation for the validity of the measurements

A pilot run of the experiment should be conducted using a fictitious task to test the procedure and demonstrate to participants how to fill out the pro-forma profile

Execution of the task under analysis.

Complete the pro-forma profile created earlier. Participants assign a rating between 0 and 1 for each of the MWL dimensions hypothesized by the Wickens model.

The analyst is responsible for extrapolating the overall workload of each task by analyzing the collected data.

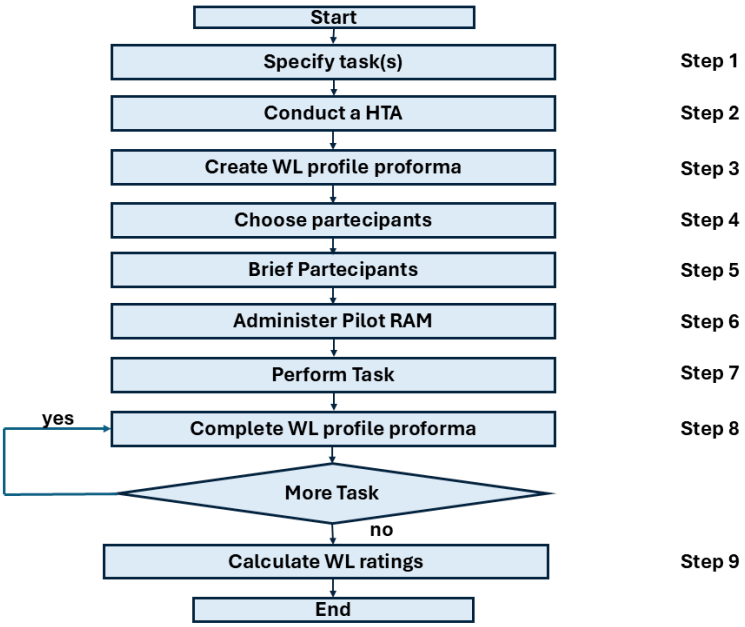

Figure 2.6: Workflow representing the various steps in the Workload Profile test

2.2.7 Performance Measures

Performance and behavioral measures are commonly used to assess mental workload by evaluating the efficiency with which an operator completes a task. Although the precise relationship between operator performance and workload has yet to be definitively established, it is generally acknowledged that optimizing mental workload can enhance overall performance.

These measures are typically categorized into primary and secondary task measures. Primary task measures serve as a direct indicator of performance and demonstrate high accuracy in assessing mental workload over extended periods [24]. They are closely linked to an operator's ability to execute the primary task [35]. However, a key limitation of these measures is their inability to identify the specific sources of workload variations when multiple tasks are performed concurrently. Due to this shortcoming, some researchers regard primary task measures as somewhat

unreliable when used in isolation [24]. Furthermore, primary task performance can be influenced by factors unrelated to workload [36].

To address this issue, secondary task measures are often employed as an indicator of an operator's available cognitive capacity [37]. These measures help differentiate variations in mental workload arising from different factors. However, secondary task measures also have limitations, as they may interfere with primary task performance and are typically sensitive only to substantial changes in mental workload.

2.2.8 Physiological measures

Physiological indicators of mental effort are employed to evaluate the body's physiological responses, based on the premise that as task demands increase, corresponding changes in physiological activity become evident. These responses can be assessed through various physiological systems, including cardiovascular, neurological, respiratory, oral, and ocular functions. The growing sophistication of sensor technology and advancements in stress-related signal processing have contributed to the increasing use of physiological measurements in experimental research.

Electrocardiac and cardiovascular measures

The signals most commonly used for physiological assessment are those related to the heart and cardiovascular system, particularly heart rate (HR), heart rate variability (HRV), and blood pressure (BP). It is generally understood that heart rate increases as mental workload rises. Heart rate variability measures the fluctuations in time intervals between consecutive heartbeats. Blood pressure is used less frequently than other cardiac measures, primarily due to its intrusive nature [35]. In contrast, heart rate and heart rate variability have been shown to be less intrusive and more responsive to changes in mental workload.

Respiratory measures

For respiratory signals, the most commonly used feature to assess correlations with mental workload is respiratory rate, which represents the number of breaths per unit of time. Typically, respiratory rate increases as mental workload rises. Similar to heart rate and heart rate variability, it is easy to measure and minimally invasive. Another reported indicator is oxygen consumption, which generally exhibits a positive linear relationship with mental workload.

Ocular Measures

The category of ocular measurements relies on indicators of ocular activity, including blink rate, blink duration, gaze angle, pupil size, pupil diameter, and pupillary responses [38]. Blink rate refers to the number of eye closures within a given time frame, while blink closure rate represents the total duration spent blinking [39].

A key challenge associated with these measures is the difficulty in distinguishing the effects of visual workload from those of mental workload [40]. Some studies suggest that ocular measures are primarily effective for assessing visual workload and are highly sensitive to environmental influences. For instance, pupil diameter tends to increase with higher mental workload but is also affected by various cognitive demands and emotional states. However, a significant limitation is that it becomes unresponsive under extreme cognitive overload and is highly susceptible to changes in lighting conditions.

Another widely utilized method is electrooculography (EOG), which measures the electrical potential between electrodes placed on facial muscles involved in eye movement control, providing valuable insights into ocular activity.

Oral measures

Salivary cortisol has frequently been linked to mental workload assessment and has been experimentally demonstrated to reliably reflect mental workload levels [41]. However, its use remains limited due to its primary drawback—its sensitivity, which tends to respond only to significant increases in task demands. In general, salivary cortisol exhibits low sensitivity, with minimal variation, particularly in the context of simple tasks.

Mental measures Monitoring brain activity has always been crucial in assessing MWL. Understanding how the brain works during task performance is essential because as cognitive workload increases for a particular task, the brain resources available for other, non-primary tasks diminish [42].The cognitive processing of other tasks may be delayed or impaired if brain resources fall below a certain threshold [43]. Over time, brain activity related to mental workload (MWL) has been commonly assessed using techniques such as electroencephalography (EEG), functional magnetic resonance imaging (fMRI), and functional near-infrared spectroscopy (fNIRS) [44]. However, EEG and fNIRS have gained wider adoption due to advancements in sensor technology, which have made them more portable, user-friendly, and reliable [45]. These methods offer two distinct approaches to monitoring MWL:

- **EEG** i s a technique that measures the electrical potential of the brain and represents electrically sensed signals over time that can be decomposed in the frequency domain. This signal is typically divided into four frequency bands: Δ ($< 4\,\text{Hz}$)), Θ ($4\,\text{Hz}$ to $8\,\text{Hz}$), α ($8\,\text{Hz}$ to ($13\,\text{Hz}$) and β ($13\,\text{Hz}$ to $30\,\text{Hz}$) [46]. A key feature of the EEG signal is represented by event-related potentials (ERPs), which represent small changes in brain electrical activity recorded from the scalp, triggered by internal or external events [47].

- **fNIRS** is a non-invasive tool for continuous bedside monitoring of regional tissue oxygenation. It leverages the transparency of the scalp and skull to infrared light, as well as the differing absorption spectra of oxyhemoglobin and

deoxyhemoglobin, to quantify local hemoglobin oxygen saturation in brain activity. This enables the detection of activation or deactivation in specific brain regions. [48].For instance, fNIRS assessments of the prefrontal cortex (PFC) are directly associated with working memory, decision-making, and executive control, all of which are closely linked to MWL.

Skin measures Measuring temperature across different regions of the body is another established method for assessing mental workload. For example, the Nasal-Forehead (N-F) temperature has been suggested as an effective indicator for evaluating a navigator's mental workload [49]. Ohsuga observed a decrease in skin temperature and an increase in heart rate when participants were exposed to stressful task conditions. Skin temperature serves as an indicator of peripheral sympathetic nervous system activity, which is activated by mental strain, making it a potential measure for assessing mental workload. However, a major limitation is its susceptibility to environmental temperature fluctuations. Additionally, the skin on the forehead is less responsive to different types of strain compared to the skin on the nose [50]. In addition to skin temperature, various other physiological measures have been explored as potential indicators of mental workload, including electrodermal activity (EDA) and galvanic skin conductance response. EDA can be divided into phasic and tonic components, where the tonic element represents the baseline skin conductance, while the phasic component reflects temporary increases above this baseline during task performance. Phasic signals can be further categorized into specific and non-specific responses. Specific signals arise from exposure to a distinct stimulus, whereas non-specific EDA signals exhibit a weaker association with mental workload. Some studies have observed correlations between non-specific EDA signals and operator response time. Due to these limitations, EDA has been adopted as a physiological measure in only a limited number of applications.

2.3 Photoplethysmographic signal

Among the various techniques available is photoplethysmographic (PPG) signal analysis. PPG is a particularly noteworthy optical measurement because of its noninvasive nature, which not only provides high user comfort but also allows the simultaneous acquisition of features belonging to different physiological signals. This feature minimizes the need for numerous sensors, thus improving the comfort and efficiency of data collection [51].

2.3.1 Introduction

The term "plethysmography" originates from the Greek words "plethysmos," meaning "increase," and "graph," meaning "writing." This diagnostic technique measures volume changes in blood flow within an organ or body region. Photoplethysmography, a specific form of noninvasive and cost-effective optical plethysmography, detects variations in blood volume in the skin's microvascular bed. This method relies on photometric principles, utilizing the interaction between light and biological tissue to generate a measurable signal. The system includes a light-emitting diode (LED) that illuminates the tissue and a photodiode that captures the light after it passes through the area of interest, Figure 2.7. As the emitted light interacts with the tissue, it is absorbed to varying extents by different components, such as skin pigments, bone, and venous and arterial blood. The fundamental principle is that blood absorbs more light than the surrounding tissues, enabling the assessment of hemodynamic changes.

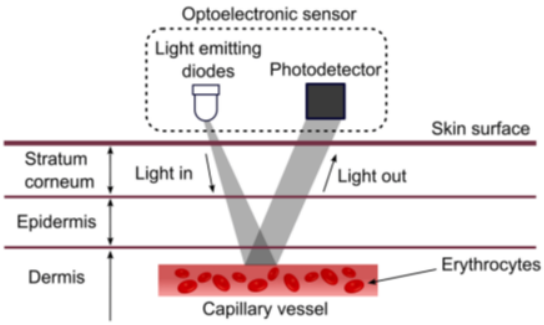

Figure 2.7: Representative diagram of how a PPG signal is acquired: light is emitted at a given wavelength and then reflected from the tissue of interest

2.3.2 Physical principles

The PPG signal is governed by the Lambert-Beer law, which describes the attenuation of light as it passes through an absorbing medium. When a monochromatic light beam with an initial intensity I_0 travels through a homogeneous material, its intensity I at the output is reduced due to absorption by the medium. If no absorption occurs, the intensity remains equal to I_0. Each material has a unique absorption spectrum, defining how it interacts with different wavelengths of electromagnetic radiation.

However, biological tissues are not homogeneous; they are composed of multiple layers with distinct and proper optical properties. Different types of tissues absorb and scatter light in unique ways, depending on their composition. The photoplethysmographic (PPG) signal can be understood by applying the Lambert-Beer

law to biological tissues, modeling them as a sequence of N optical segments, each with its own absorption characteristics. This variation in absorption enables PPG to detect dynamic changes in blood volume, which forms the foundation for physiological monitoring.

The Lambert-Beer law is expressed as in Equation 2.1:

$$I = I_0 e^{-\varepsilon l c} \tag{2.1}$$

The relationship between these variables can be expressed as follows: the intensity of the light transmitted (I) through a medium will decrease exponentially in relation to the intensity of the initially irradiated monochromatic light (I_0), the molar absorption coefficient (ε), the optical path length (l) and the concentration of the medium (c). The molar absorption coefficient, expressed in units of $\mathrm{M}^{-1}\,\mathrm{cm}^{-1}$, depends on the sample, the wavelength of light used and the chemical species determining the absorption. In the case of arterial blood, the molar absorption coefficient is modelled as a linear combination of that of oxygenated haemoglobin (HbO_2) and deoxygenated haemoglobin (Hb), as in Equation 2.2:

$$\varepsilon_\lambda = S\varepsilon_{\lambda,\mathrm{HbO_2}} + (1 - S)\varepsilon_{\lambda,\mathrm{Hb}} \tag{2.2}$$

In this context, S represents the oxygen saturation in the blood, while λ denotes the light's wavelength. The molar absorption coefficients for both oxygenated and deoxygenated hemoglobin at various wavelengths can be determined experimentally. It is the subtle difference in the absorption of light by these two forms of hemoglobin that enables the calculation of blood oxygen saturation levels.

The concentration of the sample refers to the number of moles of a substance dissolved in a liter of solution, whereas the optical path length indicates the distance the light travels through the sample. This is essentially the thickness of the material through which the light passes, measured in centimeters. The exponential term in Lambert-Beer's law is referred to as absorbance (A), which is given by Equation 2.3:

$$A = -\varepsilon l c \tag{2.3}$$

However, the direct application of this law to calculate light absorption in biological tissues requires modifications. It is essential to account for the fact that the tissues through which the light passes are not homogeneous and exhibit varying degrees of optical scattering. These tissues contain multiple absorbers (such as blood, water, and melanin) and diffusers (like collagen and keratin). As a result, the Lambert-Beer law is not directly applicable to biological media, as it does not incorporate the effects of scattering. Additionally, in a medium where only absorption occurs, the sample thickness d is equivalent to the optical path length l. However, in biological tissues, which involve both absorption and scattering, the optical path length differs from the material thickness. It is instead linked to a

factor known as the 'differential pathlength factor' (DPF), which is dependent on both the optical wavelength and the tissue's anatomical properties. A DPF value greater than 1 indicates that the optical path length within the tissue is always longer than the direct distance between the light source and the detector. The modified Lambert-Beer law, Equation 2.4 which accounts for both absorption and scattering in a medium like biological tissue, defines the absorbance (A) of light at a specific wavelength (λ) using the following equations:

$$A_\lambda = \varepsilon_\lambda l_\lambda C + G_\lambda \tag{2.4}$$

where ε and C represent the extinction coefficient and the concentration of the absorber, respectively, d denotes the distance between the source and detector, l is the optical path length, DPF refers to the 'differential path length factor,' and G is a diffusion-dependent parameter that remains constant throughout the cardiac cycle, implying that it does not change during a PPG measurement with a fixed wavelength and geometry. In the case of a heterogeneous medium containing n absorbers, the total light absorbance can be determined by summing the absorbances across the different layers, Equation 2.5:

$$A_\lambda = \sum_{i=1}^{n} \varepsilon_{\lambda,i} C_i l_\lambda + G_\lambda \tag{2.5}$$

where $\varepsilon_{\lambda,i}$ and C_i represent the extinction coefficient and concentration of the i-th absorber, respectively, while l_λ is the total optical path length through the medium.

The amount of light transmitted through the skin can then be expressed as in **??**:

$$I = I_0 e^{-\sum_k A_k} \tag{2.6}$$

In this context, total absorbance is affected by the composition and properties of the skin layers. Each skin layer contributes differently to total absorbance based on factors such as its composition, the concentration of absorbing components, light scattering properties, and thickness. The Equation 2.6 summarizes how light interacts with the skin during photoplethysmographic (PPG) measurements. Therefore, understanding the structure of the skin and how it impacts light transmission is crucial for the accurate interpretation of PPG signals, Figure 2.8. Other factors that may influence the detected light intensity include blood volume at the measurement site, arterial diameter, hemoglobin concentration, and the direction of blood flow relative to the cardiac cycle.

Light is an electromagnetic wave that is visible within the wavelength range of 400 to 700 nm. PPG devices typically utilize both visible and infrared wavelengths. Longer wavelengths are able to penetrate deeper into tissue. Red (640−660 nm)

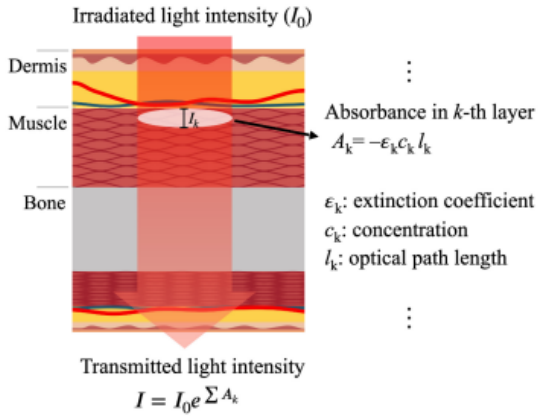

Figure 2.8: Pattern of light transmitted from one side of a portion of fabric to the other according to Lambert-Beer's law

and infrared (880−940 nm) wavelengths, in particular, offer the greatest tissue penetration, reaching subcutaneous layers, arterioles, and arteries. This makes them ideal for use in transmitters that need to pass through tissues such as a finger or earlobe. In contrast, green light (565 nm) has limited penetration, primarily passing through arterioles. As a result, green light is commonly used in reflectance-based systems. The pulsatile nature of arterial blood flow, which correlates with the heartbeat, is most pronounced with green light, making it particularly effective for heart rate detection in wearable reflectance devices.

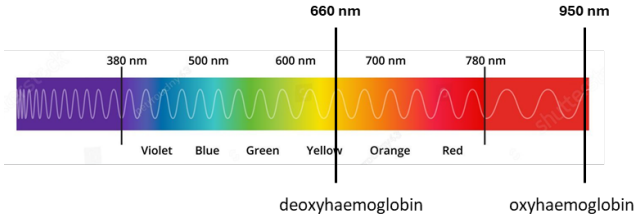

Figure 2.9: Light spectrum with the characteristic absorption wave frequencies of oxygenated and deoxygenated hemoglobin

As might be expected, the most commonly used frequencies are around 660 nm (red light) and 940 nm (infrared) Figure 2.9. This choice is made because these are the two ranges in which oxygenated and deoxygenated blood have a clearly distinguishable absorption.

In that area, the absorption is almost flat, so if there is a small inaccuracy in the wavelength of the emitter, it does not cause a large measurement error.

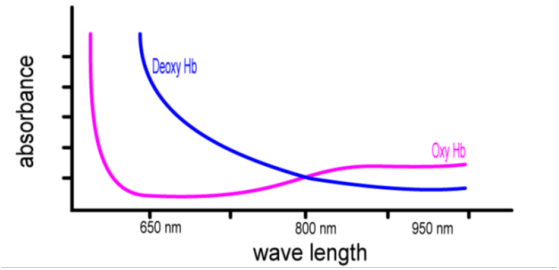

Figure 2.10: Trend of absorbance of oxygenated and deoxygenated hemoglobin as the wavelength changes

As shown in the image Figure 2.10:

- For $\lambda < 600$ nm, the light is completely absorbed by the skin.
- For $\lambda \approx 660$ nm, deoxygenated hemoglobin absorbs most of the light.
- For $\lambda \approx 950$ nm, oxygenated hemoglobin absorbs more light.

In that area, the absorption is almost flat, so if there is a small inaccuracy in the wavelength of the emitter, it does not cause a large measurement error.

2.3.3 Acquisition modes

There are two modes of operation: transmittance and reflectance. These modes depend on the relative position of the LED and the photodiode. As seen in

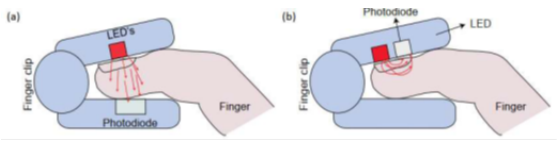

Figure 2.11: PPG signal acquisition mode: on the left, transmission mode, LED and photodiode are in opposite positions of the finger clip; on the right, reflection mode, photoemitter and photoreceptor are on the same side of the finger clip

Figure 2.11, in transmittance mode, the LED and photodiode are positioned on opposite sides of a clip. The light emitted by the LED passes through the tissue and is detected by the photodiode on the other side. This setup is generally less sensitive to motion artifacts and is commonly used in healthcare applications to measure oxygen saturation. However, a limitation is that measurements can only be taken at sites where the clip can be applied, such as the finger, toe, or earlobe.

In contrast, reflection mode involves placing the LED and photodiode on the same side, just a few millimeters apart. The LED illuminates the fabric and the photodiode detects its scattered light. Reflective devices can be applied to a wider range of body parts, making them ideal for use in wearable devices offering greater flexibility for continuous monitoring in various body regions.

2.3.4 PPG signa waveform

The PPG signal is composed of two main components: the pulsatile (AC) component and the non-pulsatile (DC) component.

1. **Pulsatile (AC) Component** reflects how blood volume changes in sync with each heartbeat and is mainly associated with the systolic phase of the cardiac cycle, when the heart contracts and pumps blood into the arteries. The alternating current (AC) component is crucial for providing insights into heart rate, heart rate variability, and other cardiovascular parameters, offering valuable information for assessing cardiovascular health and performance.

2. **Non-pulsatile (DC) Component** The DC component reflects the baseline level of light absorption, which is associated with static blood volume and the inherent properties of the tissue. This component depends from factors such as the average blood volume in the tissue, skin pigmentation, and the presence of other tissues and bone. While the direct current (DC) component is less dynamic compared to the AC component, it still provides valuable information about overall tissue perfusion, offering insights into the general health and circulation of the tissues.

The PPG signal is periodic and synchronized with the ECG, as each heartbeat generates a pressure wave that propagates through the blood vessels, resulting in an increase in their volume. The rise in blood volume during systolic contraction leads to greater light absorption, which causes a decrease in the light intensity detected by the photodiode. For more effective analysis, it is often preferred to work with a PPG waveform that mirrors the corresponding arterial pressure waveform, with a peak during systole and a trough during diastole. To achieve this, the light intensity signal detected by the photodiode is inverted so that it becomes proportional to light absorption. Figure 2.12.

This results in a waveform, as shown in figure Figure 2.13, which can be divided into an anacrotic (upstroke) and dicrotic (downstroke) limb. The waveform is characterized by two key phases: the systolic phase,when the heart pumps blood out from the left ventricle following the opening of the aortic valve, marked by a rapid pressure increase followed by a decline, and the diastolic phase, during which

Figure 2.12: Difference in morphology between a signal in transmittance and one in absorbance. It is preferred to have a signal synchronous to the ECG signal

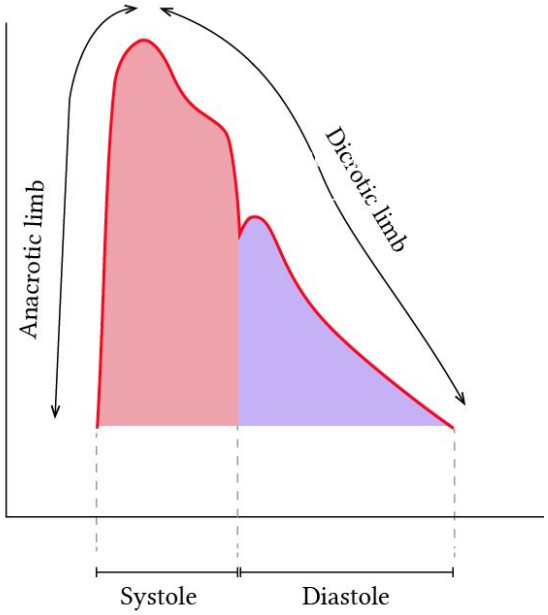

Figure 2.13: Typical waveform of the PPG signal, with the division between the systolic and diastolic components

blood flows into the peripheral circulation. These two phases are separated by the dicrotic notch, which indicates the closure of the aortic valve.

By examining the specifics of the pulse wave, the shape of the PPG signal can be studied to extract different physiological parameters. As shown in Figure 2.14 a typical PPG waveform consists of the following main components:

- **Systolic upstroke**:The systolic upstroke represents the initial, rapid rise in the pulse waveform, which corresponds to the quick increase in arterial pressure

as the left ventricle ejects blood into the aorta during systole. This phase is marked by a steep incline in the waveform, signifying robust ventricular contraction and effective blood flow.

- **Systolic peak**: The systolic peak is the highest point of the pulse waveform, reflecting the maximum arterial pressure reached during systole. This peak serves as a vital indicator of cardiac output and vascular health, as it marks the point of maximal blood ejection from the heart.

- **Systolic decline**: Following the systolic peak, the systolic decline marks the phase where arterial pressure begins to drop. This downward trend indicates the gradual reduction in pressure as the heart transitions from contraction to relaxation, signaling the end of blood ejection.

- **Dicrotic notch**: the dicrotic notch is a small, distinct downward deflection limb of the pulse waveform on the descending. It results from the closure of the aortic valve, signifying the transition from systole to diastole. This feature plays a crucial role in accurately identifying the timing of valve closure.

- **Diastolic decay (or runoff)**: diastolic decay refers to the progressive decline in arterial pressure following the dicrotic notch, As blood flows into the peripheral circulation, this phase of the waveform illustrates the progressive decrease in pressure during the heart's relaxation period, eventually returning to baseline levels.

- **End-diastolic pressure**: End-diastolic pressure is the lowest point on the pulse waveform, occurring immediately before the onset of the next cardiac cycle. It represents the minimum arterial pressure within the cardiac cycle and serves as a key indicator of baseline vascular tone and overall cardiovascular health.

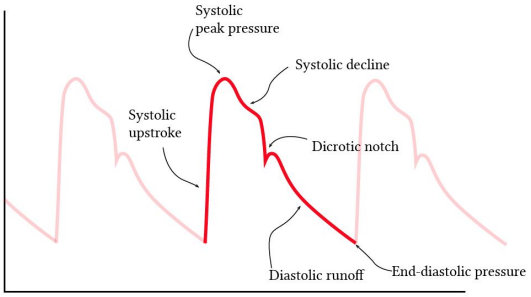

Figure 2.14: PPG wave with all its characteristic points

The frequency content of the PPG signal is similar to that of blood pressure, although the waveform exhibits different characteristics. It is generally recommended to use a sampling frequency of at least 100 Hz with a resolution of 10 bits or greater. The waveform can vary depending on factors such as the measurement location, the subject's age, heart rate, ejection volume, and pressure levels.

The signal can be degraded by sudden movements (common when measuring at the fingertip), as in the examples shown in the figure below.

2.3.5 Interaction between respiration and circulation

Respiration and circulation are intricately linked. Variations in intrathoracic pressure caused by breathing directly influence the central veins. During inspiration, venous pressure decreases, leading to an increase in venous return. This results in a rise in the filling pressure of the right ventricle, which, in turn, increases the right ventricular ejection volume. As blood accumulates in the lungs, the left ventricular ejection volume decreases. Consequently, systolic blood pressure drops, as does diastolic pressure, although to a lesser extent, while heart rate increases. During expiration, the flow of blood to the left side of the heart rises, leading to an increase in left ventricular ejection volume. At the peripheral level, both arterial and venous pressures increase.

In the case of positive pressure ventilation, the effects on circulation are reversed. Respiratory-induced variations in blood volume are observed both at the arterial and venous levels, with the changes being more pronounced in the right heart and, especially, in left ventricular ejection volume. These variations can also be detected in the pulmonary circulation. For example, the transmural pressure in the right heart varies by 32%, whereas the mean arterial pressure in the carotid artery fluctuates by only 2%. The venous side of the circulatory system, which contains the largest volume of blood and is under low pressure, is particularly sensitive to small pressure changes. Most of the blood in the skin's circulation is stored in the venous plexus, and blood flow in the dermis is regulated by vasoconstriction, mediated by the sympathetic nervous system.

Arteriovenous anastomoses, located at distal points, are densely innervated by the sympathetic nervous system. Sympathetic efferent activity in the skin remains synchronized with respiration, even during periods of apnea. Although the sympathetic contribution to the respiratory PPG signal is relatively small compared to the more dominant changes in venous return and cardiac ejection volume, it still plays a role. Another noteworthy phenomenon in the interaction between respiration and circulation is "entrainment" or "phase locking." This refers to the process where an oscillating system synchronizes with the frequency of another oscillator. In this context, changes in blood flow driven by respiration can align with the heartbeat, resulting in periodic fluctuations in the PPG signal that are

tightly coupled to the respiratory cycle.

2.4 Estimation of respiratory rate from PPG signal: State of the art

The methods used to extract respiratory rate from the PPG signal can broadly be categorized into **digital filter-based techniques** and **decomposition-based techniques**. The primary distinction between these approaches is that digital filter-based techniques are relatively straightforward to implement and, due to their minimal impact on the signal, they incur lower computational costs. This makes them a suitable choice for real-time data acquisition and processing. In contrast, decomposition-based techniques tend to be more resilient to common challenges in PPG signals, such as motion artifacts.

The following outlines the techniques associated with each type of frequency extraction method for PPG signals.

2.4.1 Digital Filter-Based Techniques

- **IIR and FIR Filters** [52]:
  - **FIR Filter:** The output of an FIR filter depends solely on the current and previous inputs. This characteristic enables FIR filters to maintain a linear phase response, meaning they do not alter the waveform of the signal, thereby ensuring minimal distortion. As a result, FIR filters tend to be more stable, Equation 2.7.

$$y[n] = \sum_{k=0}^{M} h[k]\, x[n-k] \tag{2.7}$$

    where:
    - $y[n]$ is the filter output at the time n
    - $x[n]$ is the filter output at the time n
    - $h[k]$ is the filter impulse response (the filter coefficients)
    - M is the filter order, which determines the number of coefficients
  - **IIR Filter:** An IIR filter incorporates feedback, meaning that the output depends not only on the current and previous inputs but also on past outputs. This feature allows for more efficient responses with a lower filter order, thus requiring fewer coefficients than an FIR filter to achieve similar results. However, the use of feedback can introduce distortion into the signal, potentially compromising stability. As a result, FIR filters are

typically preferred when signal stability is crucial, while IIR filters are often chosen when computational resources are constrained and higher frequency precision is needed, Equation 2.8.

$$y[n] = \sum_{k=0}^{M} b[k]\, x[n-k] - \sum_{k=1}^{N} a[k]\, y[n-k] \tag{2.8}$$

where:

* $y[n]$ is the filter output at the time n
* $x[n]$ is the filter intput at the time n
* $b[k]$ are the self-response coefficients (for inputs)
* $a[k]$ are the output response coefficients (for past outputs)
* M is the filter order for the input section
* N is the filter order for the output part

- **Autoregressive Filter (AR):** An autoregressive (AR) filter is a statistical model commonly used for analyzing and forecasting time series data. In an AR filter, the current value of a variable is linearly dependent on its previous values and an error term. AR filters are particularly useful for signals that display short-term linear dependencies, making them ideal for modeling and predicting such patterns in time-series data, Equation 2.9 [53]

$$x(n) = \sum_{k=1}^{p} a_k x(n-k) + e(n) \tag{2.9}$$

where:

  – a_k is the coefficient for each term in the summation,
  – $x(n-k)$ is the delayed input signal at time $n-k$,
  – $e(n)$ is the error or disturbance term at time n.

- **Adaptive IIR Notch Filter:** An adaptive IIR (Infinite Impulse Response) notch filter is a specialized IIR filter designed to attenuate or eliminate specific unwanted frequencies from a signal. This filter is particularly effective when the interfering frequency fluctuates over time and is not predetermined. Using adaptive algorithms, such as the **Least Mean Squares (LMS)** method, the filter continuously adjusts its coefficients to track the variations in the signal. Once the undesired frequency is detected, it is either removed or significantly reduced, creating a "notch" in the frequency spectrum [54]

2.4.2 Techniques based on signal decomposition

Decomposition techniques are methods used to break down a signal into its individual components, making it easier to analyze and extract information from each part. These techniques are particularly useful for analyzing noisy signals, as they allow for the separation of noise from the underlying signal. However, it is important to note that decomposition methods generally come with a higher computational cost, which makes them less suitable for real-time processing compared to digital filter-based techniques. This is because decomposition techniques tend to be slower in processing the signal.

- **Wavelet Transform**

  The wavelet transform is a signal analysis method that enables the simultaneous examination of both frequency and amplitude variations of a signal in the time-frequency domain. This approach is particularly effective for analyzing non-stationary signals, which are signals whose frequency content changes over time. A wavelet is a waveform of finite duration, characterized by concentrated oscillations over time, a zero mean value, and non-zero energy.

  The continuous wavelet transform is defined as in Equation 2.10:

$$T(a,b) = \frac{1}{\sqrt{a}} \int_{-\infty}^{+\infty} x(t) \Psi^* \left(\frac{t-b}{a} \right) dt \tag{2.10}$$

  where:

  - Ψ^* is the complex conjugate of the wavelet function,
  - b is the location parameter of the wavelet,
  - a is the dilation parameter of the wavelet.

  The dilation parameter a has the following properties:

  - If $a < 1$, the wavelet is compressed, and details change rapidly, corresponding to high frequencies.
  - If $a > 1$, the wavelet is dilated, and details change slowly, corresponding to low frequencies.

  By applying the wavelet transform, two bands are obtained, Figure 2.15:

  - Band B, which contains the information of interest, is called the *primary band*.
  - Band A contains relevant features.

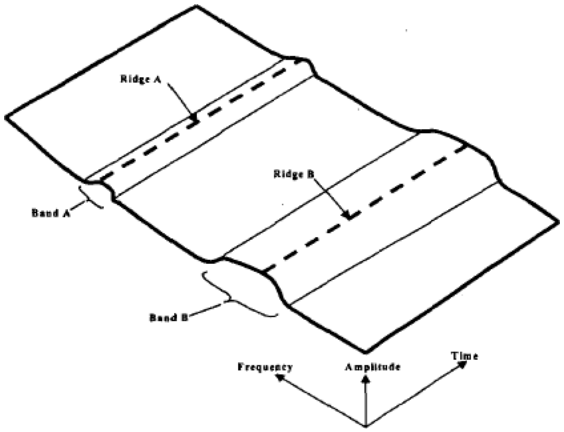

Figure 2.15: Visualization of A and B bands after decomposition by wavelet Transform

If the signal contains noise or other erroneous characteristics with spectra similar to those of the B-band, it may obscure the information within the B-band.

To improve the analysis, a second wavelet transform is applied to Band A. This band is then decomposed into the RAP and RFP signals. From the RFP signal, the period of its variations is determined and subsequently converted into the corresponding respiratory frequency [55].

- **Principal Component Analysis (PCA)** Principal Component Analysis (PCA) is a statistical technique used to analyze datasets where multiple dependent variables are used to describe each observation. The primary goal of PCA is to represent these variables with a new set of orthogonal variables, known as principal components, which highlight the significant underlying information within the dataset [56].

  An additional advantage of PCA is that it allows for the compression of the dataset size while preserving much of its information content, thereby simplifying subsequent processing. The foundation of PCA is based on maximizing variance and ensuring orthogonality. The first principal component is selected to capture the maximum variance and, therefore, the most significant amount of information. Each subsequent component is chosen to be orthogonal to the preceding components, with the aim of capturing the maximum possible variance that remains [57]. It is important to highlight that techniques such as PCA have been thoroughly explored in the field of signal processing for extracting key variables from a given signal or multiple signals. These methods have also found applications in the biomedical domain, particularly for

extracting vital parameters from radar data, as outlined in [58].

2.4.3 Empirical Mode Decomposition (EMD)

Similar to wavelet analysis, Empirical Mode Decomposition (EMD) is a method used to decompose non-stationary and non-linear signals into a series of intrinsic mode functions (IMFs), which are mono-component signals representing oscillations at various resolution scales.

An IMF is a function that captures the oscillation mode inherent in the data signal. Unlike wavelet analysis, where a predefined mother wavelet is chosen before the analysis, EMD extracts the basis functions (IMFs) directly from the data. This feature allows the IMFs to more accurately represent the local characteristics of the signal and adapt to its oscillatory patterns over time.

A signal $y(t)$ can be represented as the sum of a set of IMFs plus a residual, Equation 2.11:

$$y(n) = \sum_{k=1}^{N} s_k(n) + r_k(n), \quad k = 1, 2, \ldots, N \tag{2.11}$$

where:

- $s_k(n)$ are the resulting IMFs,
- $r_k(n)$ is the residual term.

For each intrinsic mode function (IMF), the frequency peak with the highest power is identified. Respiratory modulation is then estimated by summing the IMFs whose peak frequencies fall within the respiratory frequency range.

A significant challenge in Empirical Mode Decomposition (EMD) is the phenomenon known as mode mixing. This occurs when different signals, which should ideally be separated into distinct modes (IMFs), are instead combined into a single mode, or conversely, when a single mode contains oscillations from multiple time scales or frequencies.

To address these issues, several improvements and variations of the EMD have been proposed, such as the Extended EMD (EEMD) and Complete EEMD (CEEMD). These methods aim to reduce the impact of mode mixing by introducing Gaussian noise or altering the decomposition process, thereby enhancing the accuracy of signal separation.

Chapter 3

Materials

3.1 BiosignalplusX

Biosignalsplux is a versatile, multi-sensor platform designed specifically for biosignal acquisition in research and development (RD) environments. One of the primary challenges in RD projects is obtaining high-quality biosignal data from various sensors simultaneously, and Biosignalsplux addresses this need by providing a comprehensive solution for gathering diverse physiological measurements, ensuring both accuracy and reliability in data collection [59].

3.1.1 Biosignalplus Platform

The BiosignalPlux device supports the simultaneous acquisition of multiple biosignals through its 8-channel toolkit, allowing the use of up to eight sensors concurrently. This capability ensures the collection of high-quality, wireless signals without limitations. With a sampling rate of 3,000 Hz and a resolution of 16 bits per channel, the device can record up to 10 hours of data. Additionally, the video synchronization add-on allows for the recording of video during data acquisition, providing a synchronized view of all captured signals alongside the video. This feature is particularly useful for post-acquisition analysis, such as motion analysis, enabling a comprehensive assessment of the data, Figure 3.1

Figure 3.1: 8-Channel biosignalsplux hub dimensions

3.1.2 Sensors

The following sensors can be utilised by the device. The technical specifications of these sensors, which are directly concerned with the cardiac and respiratory analysis of the sensors with their respective biosignals, will also be explained. In addition, the main function of the other sensors will be described.

- **ECG Sensors:**

  This sensor, Figure 3.2 is designed to extract heart rate data and other ECG characteristics, making it suitable for research in fields such as biomedicine, biofeedback, psychophysiology, and sports science. Its low-noise ECG local differential triode configuration allows for quick implementation and non-invasive single-lead ECG data acquisition, ensuring efficient and reliable signal capture for a variety of applications.

  The raw digital sensor values received from the biosignalsplux device ranged between 0 and $2^n - 1$ where n denotes the sampling resolution), must subsequently be converted to the original unit of measurement (mV) of the sensor using the transfer function described in equation (3.1):

$$E_{\mathrm{CG}}\mathrm{mV} = \left(\frac{ADC}{2n} - \frac{1}{2}\right) \times \frac{V_{\mathrm{CC}}}{G_{\mathrm{ECG}}} \times 1000 \tag{3.1}$$

  where,

  – $E_{\mathrm{CG}}(V)$: ECG signal in Volt (V)

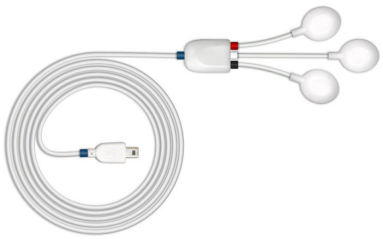

Figure 3.2: Biosignalsplux Electrocardiography (ECG) sensor

- $E_{\mathrm{CG}}(mV)$: ECG signal in milli-Volt (mV)
- ADC: aw digital value from the sensor
- n: bit resolution (default: 16-bit resolution ($n = 16$), although 12-bit and 8-bit may also be found in older versions)
- V_{CC}: Operating voltage (3V when used with biosignalsplux)
- G_{ECG}: Sensor gain (1019)

Table 3.1 shows the technical specifications of the ECG sensor:

Parameter	**Value**
Gain	1019
Range	±1.47mV (@ VCC = 3V)
Bandwidth	0.5-100Hz
Consumption	0.5mA
Input Impedance [Typical]	100GOhm
CMRR	100dB

Table 3.1: ECG Sensor Specifications

The illustration shown in Figure 3.3 show the recommended electrode placement for the acquisition of ECG signals in Einthoven configurations with electrode cable lenghts of 1.5cm (+ -) and 3 cm (reference) as those used for the experimental set-up used

- **Inductive Respiration (RIP) Sensor:**

  This sensor is particularly well-suited for dynamic environments, providing accurate measurements of respiratory parameters in various conditions. Its design helps minimize motion artifacts, making it a reliable tool for applications such as ambulatory monitoring and stress testing. By measuring the

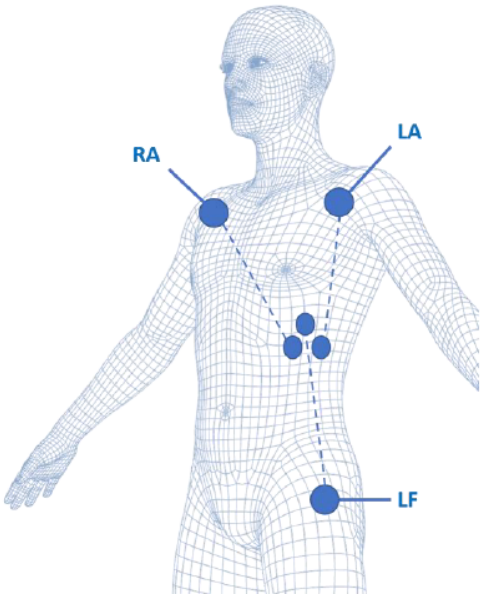

Figure 3.3: Enter Electrode placements for ECG acquisitions in Einthoven configurations using the standard ECG sensor with electrode cable lenghts of 1.5cm (+ -) and 3 cm (reference)

displacement of the chest or abdomen, it gives insight into respiratory patterns, which is valuable for evaluating respiratory health, cycle regularity, and other related parameters, Figure 6.4, the sensor output is dimensionless and varies between ±50% and indicates how far the sensor shifts from full scale. The transfer function is given in Equation 3.2.

$$\text{RIP}(\%) = \left(\frac{\text{ADC}}{2^N} \times \frac{1}{2}\right) \times 100\% \tag{3.2}$$

Description:

- RIP(%): Displacement value in percentage (%) of full scale
- ADC: Value sampled from the channel
- N: Number of bits of the channel1

Table 3.2 shows the technical specifications of the RIP sensor:

- **Blood Volume Pulse (BVP) Finger Clip Sensor:** The Blood Volume Pulse (BVP) sensor is an optical, non-invasive device designed to monitor cardiovascular dynamics by detecting changes in arterial transparency, Figure 6.5. As blood is pumped through the arteries, they become more opaque,

Figure 3.4: Inductive Respiration (RIP) Sensor.

Type	Inductive
Output	0–3V
Consumption	1mA
Cable Length	100cm±0 5cm (customizable)
Connector Type	UC-E6 (male)
Max sensor belt length	103cm
Min sensor belt length	44cm

Table 3.2: RIP Sensor Specifications

reducing the amount of light that passes through the sensor. The BVP sensor typically features a plastic clip-on housing, making it suitable for placement on the finger. This housing contains both the light emitter (LED) and the light detector (photodiode), and it also helps minimize interference from external light sources. In transmittance mode, the BVP system operates by aligning the emitter and receptor so that the photons travel perpendicular to the photodiode's surface, ensuring accurate measurement of blood volume changes.

Table 3.3 shows the technical specifications of the BVP sensor:

- **Electrodermal Activity (EDA) Sensor:**

  The biosignalsplux EDA sensor is designed to accurately measure the electrical properties of the skin, specifically focusing on electrodermal activity (EDA),

Figure 3.5: Blood Volume Pulse (BVP) Finger Clip Sensor.

Gain	34
Wavelength	670nm
Bandwidth	0 02−2 1Hz
Consumption	4 8mA

Table 3.3: BVP sensor specification

also known as Galvanic Skin Response (GSR). EDA is a physiological measure that reflects the activity of sweat glands in the skin, which is influenced by the autonomic nervous system. The sensor's low-noise signal conditioning and amplification circuit ensures optimal performance, enabling the detection of even the most subtle electrodermal responses. This capability makes the sensor highly effective for monitoring autonomic nervous system activity and stress responses (Figure 3.6).

- **Functional Near-Infrared Spectroscopy (FNIRS) Sensor:**

  The FNIRS (Functional Near-Infrared Spectroscopy) sensor is a user-friendly device that utilizes two emitting LEDs, one in the red region and the other in the infrared region of the light spectrum, to measure light reflectance in cortical tissue. This non-intrusive and non-invasive sensor is designed to estimate local oxygen saturation levels in the blood, providing insights into the activity of perfused tissue. It is particularly useful for tracking brain activity by measuring variations in oxygen saturation levels within specific brain regions.

Figure 3.6: Electrodermal Activity (EDA) Sensor

Typically, the sensor is applied to the forehead for these measurements. The reflected light from each LED is absorbed by a photodiode, and the resulting current is converted into a digital value, which is then transmitted via SPI for further analysis (Figure 3.7).

Figure 3.7: fNIRS sensor

3.1.3 Open Signals (r)evolution Software

OpenSignals is a comprehensive software platform designed for real-time visualization of biosignals, fully compatible with all PLUX devices. It offers essential features such as simultaneous sensor data acquisition from multiple channels and devices, real-time visualization, and data logging. Additionally, OpenSignals provides a suite of tools for data analysis, enabling users to generate reports directly from the recorded data and extract features from the signals without the need for programming. This makes it an ideal solution for researchers and practitioners in various fields who require efficient biosignal processing and analysis.

Among the various features the software offers users:

- Reliable acquisition and visualisation of biosignals.
- Offline visualisation of data.
- Automatic sensor detection.
- Export of sensor data in .TXT, .H5 and .EDF formats (example signals and files available).

3.2 Capnobase Dataset

The following section describes the dataset 'Capnobase' used to test the algorithm and provides an initial assessment of its performance against the respiratory rate obtained by the research team using the Smart Fusion algorithm. Details of the dataset from an engineering perspective are examined in the next section.

3.2.1 Capnobase Dataset

The method used for the test phase is 'Capnobase', a benchmark which can be downloaded from the online database CapnoBase.org [60]. The dataset comprises physiological recordings collected from a total of 42 individuals, including 29 pediatric patients (average age: 4.8 ± 5.4 years, weight: 18.5 ± 23.4 kg) and 13 adult participants (average age: 46.3 ± 9.0 years, weight: 73.5 ± 24.2 kg). These measurements were obtained while the subjects were under general anesthesia at British Columbia Children's Hospital and St. Paul's Hospital in Vancouver, BC. The signals are available in both .mat and .csv format, making it easy and quick to import them into the MATLAB software framework (Mathworks, Natick,MA, USA) on which the algorithm was then developed.All participants were assessed following a study protocol approved by the institutional Ethics Committee. The recorded signals included ECG at a sampling frequency of 300 Hz, CO and airflow

at 25 Hz, and PPG at 100 Hz. Data acquisition was carried out using the S/5 Collect software (Datex-Ohmeda, Finland) with an overall sampling rate of 300 Hz, where signals originally sampled at lower frequencies (PPG, CO, and airflow) were automatically upsampled. For each patient, an 8-minute segment of high-quality recording was selected, capturing either spontaneous or controlled breathing. The CO waveform was used as the gold standard reference for determining respiratory rate (RR). A research assistant manually labeled each breath in the capnogram (with airflow support) and identified the pulse peaks in the PPG (in conjunction with the ECG). This process allowed for the validation of the derived instantaneous reference RR and heart rate (HR).

Chapter 4

Description of the Algorithm

The subsequent section delineates the algorithms implemented for the extraction of cardiac and respiratory features from the PPG signal acquisition, Figure 4.1. The initial step in this process entails the separation of respiratory and cardiac information from a given signal through the application of filtering techniques at specific and suitable frequencies. Subsequent to the separation of the signals, a processing procedure is initiated, which continues until the identification of features that are deemed to be pertinent for the study of cognitive load levels. The robustness of the algorithms is then compared with respect to the features extracted by processing the reference signals, i.e. the cardiac and respiratory signals.

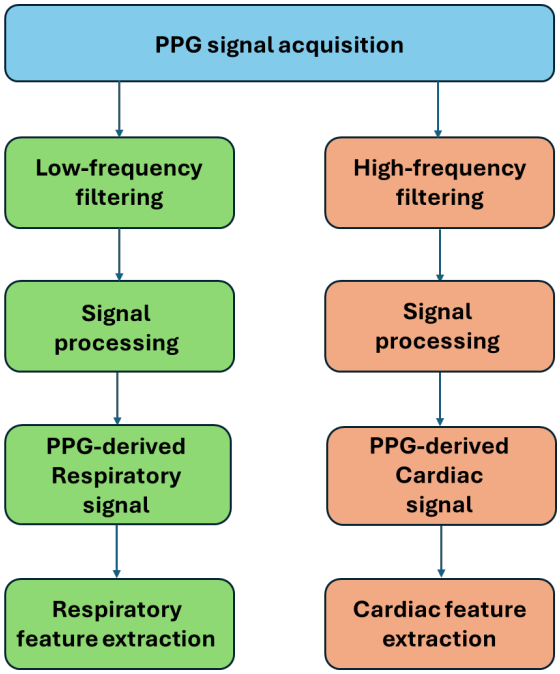

Figure 4.1: Flowchart illustrating the processing pipeline for PPG signal acquisition and processing.

4.1 Respiratory algorithm: Preprocessing

4.1.1 Filtering:

To isolate the respiratory component from the raw PPG, a low-pass butterworth filter with a cutoff frequency set at 0.7 Hz is applied, Figure 4.2. The order selection is optimised through the MATLAB function 'buttord', with a cutoff frequency set to 0 7, a stopband frequency of 1 2, a maximum allowable attenuation in the passband set to 1 dB, and a minimum attenuation in the stopband set to 20 dB.

Due to the too low frequencies of interest, it was decided not to use a high-pass filter to avoid distorting the signal

4.1.2 Smoothing function

The fenestration of the signal into smaller segments can lead to distortion of the signal in transients (at the beginning and end of the window), **??** - 4.4. This occurs because the implemented filter fails to function properly due to the sudden variations in the truncated signal. Outlier detection is performed by setting a threshold based on the mean and standard deviation of the signal. The identified

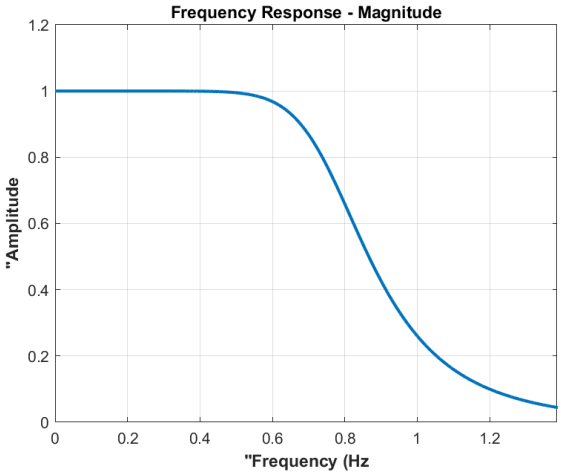

Figure 4.2: Magnitude response of the filter, showing how the amplitude varies across different frequencies

outliers are then replaced with the threshold value.

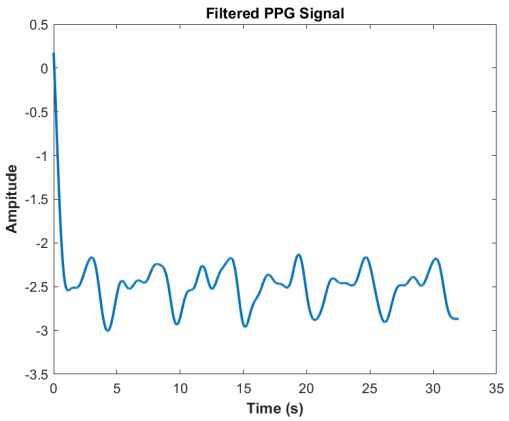

Figure 4.3: Filtered PPG with outliers problem in transients

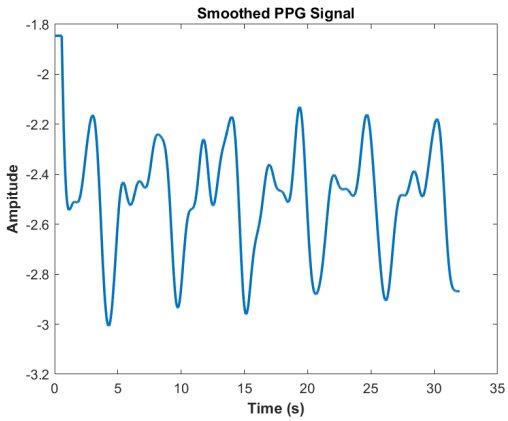

Figure 4.4: Smoothed PPg signal

4.1.3 Amplitude modulation function

Subject movement can introduce artefacts into the signal, altering the signal with peaks much higher than normal. Recognizing these changes is important to avoid errors in data interpretation, Figure **??** - Figure 4.6. An exponential amplitude modulation function is applied to selectively adjust the highest and most isolated

peaks in the signal. The exponential factor, determined empirically, is set to 0.3.

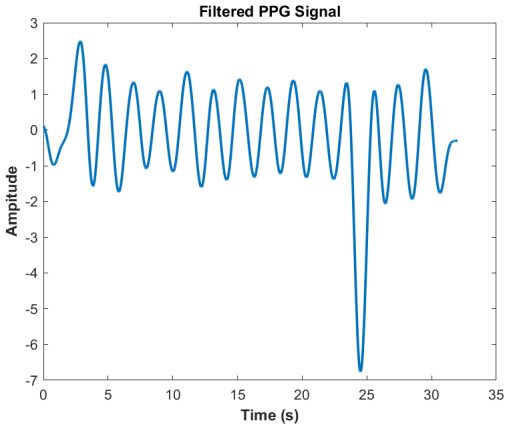

Figure 4.5: Filtered PPG with outliers problem in transients

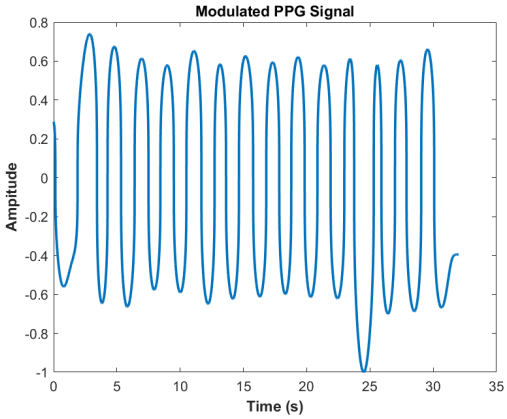

Figure 4.6: Smoothed PPg signal

4.2 Respiratory algorithm: Processing

4.2.1 Signal Quality Index (SQI)

In order to achieve signal diversification, a signal quality index is employed to determine the most appropriate processing strategy. This index returns an output value of 0, 1, or 2, depending on the signal's conformity. These values are derived through statistical analysis of the signal, specifically by calculating the kurtosis and Shannon entropy for each window using Equation 4.1:

$$H(X) = -\sum p(x) \log_2 p(x) \tag{4.1}$$

where:

- $p(x)$ is the probability of each event x in the distribution.
- The logarithm is base 2 ($\log_2$), so the unit of measurement for entropy is the bit.

Kurtosis is a measure of the peakedness of a unimodal distribution curve. That is to say, it indicates the extent to which the values within a dataset cluster around the mean, as well as the frequency of occurrence of values that are either extremely high or low. The kurtosis is defined as in Equation 4.2:

$$\kappa = \frac{\mathbb{E}[(X - \mu)^4]}{\sigma^4} \tag{4.2}$$

where μ is the mean of X, σ is the standard deviation of X, and $\mathbb{E}$ represents the expected value of the quantity $(X - \mu)$. When the curve is high, this indicates that the data are concentrated around the mean, with the presence of extreme values (i.e. heavy tails). Conversely, when the curve is low, this indicates that the data are more dispersed around the mean, but that extreme values are low (i.e. light tails).

Shannon Entropy (SE) serves as a quantitative measure of uncertainty or information content within a random variable. It evaluates the divergence of a signal's probability density function (PDF) from a uniform distribution, thereby offering an objective assessment of the uncertainty embedded in the signal.

In statistical mechanics, entropy is a fundamental concept representing the degree of randomness or disorder within a system. Higher entropy indicates greater unpredictability in observed events, reflecting an increased level of randomness in the data distribution. Conversely, when entropy is low, the system exhibits greater predictability due to the dominance of specific events that shape the distribution, effectively reducing overall uncertainty.

The kurtosis and shannon entropy values calculated for each segment are compared with threshold values taken from the literature. In the study by n. Selvaraj, the optimal threshold values were identified by testing on 350 clean signal segments and on corrupted segments with varying levels (10-50%) of added artefacts. the values are considered optimal by comparing the specificity and sensitivity of the analyses performed with these same values. For kurtosis the optimal value is 3.5 and for Shannon entropy the optimal value is 0.8 [61]. Once the thresholds have been identified, it is possible to assess how clean the signal is or is not by initialising a variable, count, equal to 0, and setting the conditions:

if $K > 3.5$ **then**
    $count = count + 1$
end if
if $SE < 0.8$ **then**
    $count = count + 1$
end if

where K is the kurtosis value of the analysed segment and SE is the Shannon entropy value.

The value of the count variable corresponds to the SI index at the output of the function.

- A value of 0 corresponds to a situation where the signal is very clean
- A value of 1 means that the signal is generally clean
- A value of 2 means that the signal is distorted by noise and it is not easy to determine which is the correct respiratory frequency

4.2.2 Respiratory Rate evaluation

The processing phase involves a different analysis depending on the resulting quality index.

- **SQI=0** The frequency is identified by parametric spectral estimation. this is carried out using the matlab pwelch function. A half-segment long window with 50% of overlap is used. For the correct spectral resolution the adequate number of point is calculated using Equation 4.3 - Equation 4.4:

$$N_{\mathrm{FFT}} = \frac{F_c/2}{\frac{1}{60}} \times 2 \tag{4.3}$$

$$\exp = \lceil \log_2(N_{\mathrm{FFT}}) \rceil \tag{4.4}$$

- **SQI=1** A noisy signal can be expected. A decomposition tecnique called Empirical Mode Decomposition (EMD) is used to process the analized segment. The EMD decomposes the signal into Intrinsic Mode Functions(IMFs) plus a residual, Equation 4.5:

$$x(t) = \sum_{i=1}^{n} \mathrm{IMF}_i(t) + r_n(t) \tag{4.5}$$

  where:

  - x is the surrogate signal
  - IMF is the single oscillation
  - r is the residual

  Intrinsic Mode Functions (IMFs) represent the fundamental oscillatory components of a signal, providing the most intuitive and interpretable decomposition. Spectral analysis, performed using the pwelch algorithm, is employed to identify IMFs that encapsulate respiratory-related information. By summing these selected IMFs, a reconstructed approximation of the respiratory signal is generated. A further Spectral analysis to select the adequate respiration rate is needed

- **SQI=2** When the SQI is 2, the signal is expected to be heavily corrupted, making it difficult to determine whether respiratory information is present. To prevent inaccurate respiratory rate estimations, the corresponding time window is excluded from analysis

For a quality index of 0 or 1, the respiratory frequency is determined through frequency analysis. Relevant peaks within the respiratory band (0.1 Hz to 0.7 Hz are identified, and among them, the lowest frequency peak is selected. This choice is based on the assumption that the fundamental respiratory frequency typically corresponds to the lowest component in this range, while higher frequency peaks are likely due to harmonics or noise.

4.2.3 Frequency check system

To enhance the robustness of the algorithm and prevent inaccurate estimations, data recording begins only after detecting two consecutive windows with an SQI of 0.

Given the quasi-periodic nature of the respiratory signal, each subsequent window is analyzed in comparison with the previous one. If the identified frequency is within an acceptable range, it is considered valid. Conversely, if it deviates significantly from the previous value, the presence of a peak close to the expected frequency is checked. If such a peak exists, it is selected as the correct one; otherwise, the estimate is deemed unreliable, and the value is replaced with NaN. If NaN values are present in the two preceding windows, the comparison is performed using the frequency calculated in the initial two windows.

4.3 Respiratory algorithm: Feature Extraction

After the correct frequency evaluation, features correlated with the level of mental workload are individuated. The respiratory features selected for the mental workload monitoring are:

- **Respiratory Rate** : the respiratory rate represents the total number of breaths taken per minute;
- **Inhalation time** : the inhalation time refers to the time taken to inhale air into the lungs. It is determined as the difference in sample positions between a peak (end of inhalation) and the preceding valley (beginning of inhalation);
- **Exhalation time** : the exhalation time indicates the duration of exhalation, or the time required to expel air from the lungs.It is calculated as the difference in sample positions between a valley (end of exhalation) and the preceding peak (beginning of exhalation);
- **Amplitude** : the amplitude describes the intensity or volume of air inhaled or exhaled. After normalizing the signal between 0 and 1, the amplitude is calculated as the difference in magnitude between a peak and the subsequent valley;

- **Ventilation** : the ventilation denotes the total volume of air inhaled or exhaled by the lungs over a specific time period. It is defined as the product of amplitude and respiratory frequency.

For each feature except for Respiratory rate, statistical measures such as mean, and standard deviation were computed (Table 4.1):

Signal	**Feature**	**Expected trend**
	Respiratory Rate	↑
	Mean Inhalation time	↓
	St. Dev. Inhalation time	-
	Mean Exhalation time	↓
rPPG	St. Dev. Exhalation time	-
	Mean Amplitude	↓
	St. Dev. Amplitude	-
	Mean Ventilation	↑
	St. Dev. Ventilation	↑

Table 4.1: Respiration feature extracted from PPG and Expected Trends

Chapter 5

Description of the Algorithm: Cardiac Component

5.1 Preprocessing

5.1.1 Filtering

After segmenting the signal, a band-pass filter is applied to isolate the cardiac component while attenuating high-frequency noise and low-frequency interference. The band-pass filter is implemented as a cascade of a high-pass Butterworth filter with a cutoff frequency of 0.5 Hz and a low-pass Butterworth filter with a cutoff frequency of 1.5 Hz. Both filters are designed with a third-order configuration.

5.1.2 Processing: Wave extraction

The subsequent step, prior to extracting cardiac features, involves identifying the correct waveform components in 10 seconds windows. This process is based on detecting the positions of local minima. By analyzing these points (Figure 2.14), it is possible to assess whether a waveform is free from artifacts and suitable for further processing or if it is corrupted and should be excluded from subsequent analyses (Figure 5.1 - Figure 5.2).

From the selected waves, characteristic features are extracted to identify the relevant cardiac properties, which are outlined below:

- **Peak position**
- **Peak height** (mV)

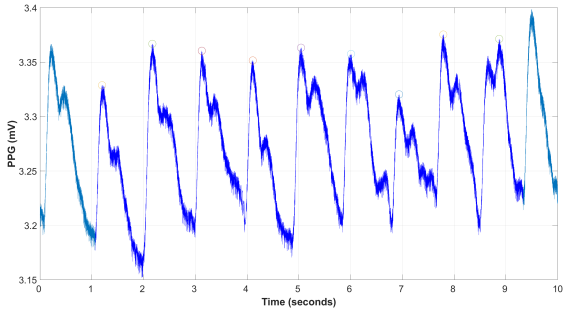

Figure 5.1: An example of the waveform extraction, where correctly identified waves are highlighted in dark blue, indicating their suitability for further processing

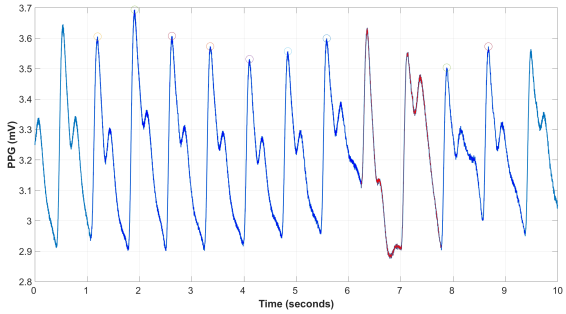

Figure 5.2: An example of the waveform extraction. Corrupted waves, deemed unsuitable for analysis, are marked in red

- **Duration** (s)
- **Rise time**(s)

5.2 Cardiac algorithm: Feature Extraction

The information extracted from artifact-free waves undergoes further processing to derive cardiac features, which enable the assessment of mental workload levels. During this phase of post-processing, a total of 19 features were derived. These features, outlined in Table 5.1-Table 5.2 - **??**, capture various characteristics of the PPG waveform, of the heart rate and of the heart rate variability, specifically its :

- **Amplitude**: the amplitude corresponds to the variation between the peak and trough values of the PPG signal within a single cardiac cycle;
- **Duration**: the duration refers to the complete time span of a PPG cycle, measured as the interval between the onset of one PPG wave and the beginning of the subsequent wave;

- **Rise time**: the rise time represents the duration required for the signal to transition from its minimum to its maximum value within a single PPG cycle;
- **Beats per minute(BPM)**: BPM (Beats Per Minute) represents the count of heartbeats occurring within a one-minute interval;
- **pNN50**: the pNN50 is the percentage of consecutive RR intervals (the time between two successive heartbeats) where the difference from the previous interval exceeds 50 ms;
- **Power of low-frequency band (PLF)**: the PLF reflects the spectral energy within the frequency range of 0.04 Hz to 0.15 Hz;
- **Power of high-frequency band (PHF)**: The PHF denotes the spectral energy within the frequency range of 0.15 Hz to 0.4 Hz;
- **PLF-to-PHF ratio**: It is the ratio of the power observed in the low-frequency band (PLF) to that in the high-frequency band (PHF).

For each feature, statistical measures such as mean, median, and standard deviation were computed.

Signal	**Feature**	**Expected trend**
PPG	Mean amplitude	↑
	St. Dev. amplitude	-
	Median amplitude	↑
	Mean duration	↓
	St. Dev. duration	-
	Median duration	↓
	Mean rise time	↑
	St. Dev. rise time	-
	Median rise time	↓

Table 5.1: PPG Features and Expected Trends

Signal	Feature	Expected trend
HR	Mean BPM	↑
	St. Dev. BPM	-
	Median BPM	↑

Table 5.2: HR Features and Expected Trends

Signal	Feature	Expected trend
HRV	pNN50	↑
	Mean PLF IBI	↓
	St. Dev. PLF IBI	-
	Mean PHF IBI	↓
	St. Dev. PHF IBI	-
	Mean PLF/PHF IBI	↑
	St. Dev. PLF/PHF IBI	-

Table 5.3: HRV Features and Expected Trends

Chapter 6

Experimental Dataset

The aim of this section is to present the population, tests, and procedure characterizing the small experimental dataset used for code validation.

6.1 Test

The N-Back test is used to assess various levels of cognitive workload. It consists of two phases: the Visual Mode and the Dual Mode, each performed three times (1-Back, 2-Back, and 3-Back), with increasing difficulty at each stage. A number of 80 trials are set for each step.

In the Visual mode, Figure 6.1, a grid of nine squares is displayed on the screen, with a gray square moving to a different position every 2.25 seconds. The participant is required to press a button labeled "Position" whenever the square returns to the same location as in 1, 2, or 3 previous steps.

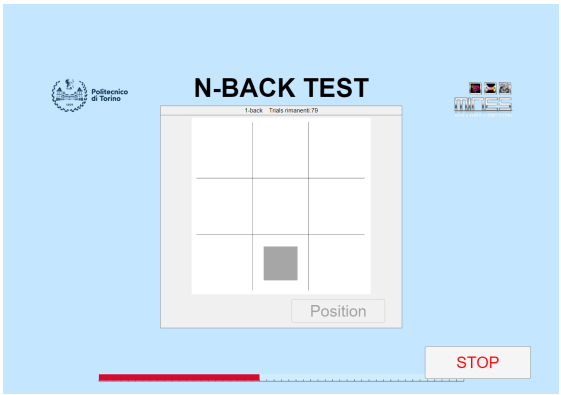

Figure 6.1: N-Back visual test graphical interface

The Dual Mode integrates both visual and auditory stimuli, Figure 6.2. In

addition to the visual task, participants listen to a sequence of letters and must press a button labeled "Audio" when they recognize the same letter that appeared 1, 2, or 3 steps earlier. This phase challenges users to process and respond to both modalities simultaneously, further increasing cognitive demand.

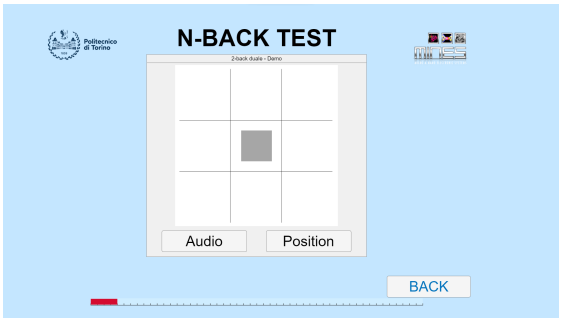

Figure 6.2: N-Back dual test graphical interface

6.2 Partecipants

The procedure was authorized by the Politecnico di Torino ethics committee (protocol number 1606). the dataset comprises 8 voluntarily selected participants divided into 9 males and 2 famales. the age range is from 21 to 27.

6.3 Equipment

8-Channel biosignalsplux Kit with its sensors is used for the acquisition of the physiological signals. In particular, the sensors used in this setup are:

- Electrocardiography (ECG) Sensor placed left rib (Figure **??**);
- Inductive Respiration (RIP) Sensor with the breathing band positioned below the pectoral line (Figure 6.4)
- Blood Volume Pulse (BVP) Finger Clip Sensor on the tip of the index finger (Figure 6.5)

Real-time visualisation and monitoring of signals is possible with Open Signals (r)evolution Software.

Figure 6.3: Demonstration figure of ecg sensor positioning.

Figure 6.4: demonstration figure of respiratory band and sensor positioning

Figure 6.5: demonstration figure of PPG sensor positioning

6.4 Procedure

This section outlines the methodology used to collect physiological signals from each participant. The entire testing process took approximately one hour to complete.

The entire procedure is divided into two phases:

- **Resting Phase** : The acquisition starts connecting the three sensors to the off-hand of the subject . Then, the volunteer is asked to sit at the desk in front of the computer and relax, avoiding unnecessary and abrupt movements to avoid corrupting the signal with movement artifacts. The rest phase lasts 5 minutes with the aim to acquire the three physiological signals that will serve as a baseline for comparison with the mental load levels under effort.

- **Testing Phase**: Before the test phase begins, participants receive a brief explanation of the procedure they will undergo, followed by a short training session in DEMO mode to familiarize themselves with the task. Six N-back tests of 80 trials each are involved in this phase. Three of them (1/2/3 Back) are only in visual mode while the others are in dual mode, visual plus audio (1/2/3 Back). A 3-minute rest phase between each test is set. The purpose of testing is to stimulate the user's mental workload by getting him involved in completing a task.

The test concluded with a final rest phase, during which participants were asked to complete two self-assessment questionnaires evaluating their perceived mental workload and stress levels. In the first form, it is asked to assign a low-medium-high level as a rating for the mental effort made.

In the second one, a ten point scale is used to classify the effort . The value it is obtained following the Bedford Scale.

The Bedford Scale is a one-dimensional assessment tool designed to measure an operator's available mental capacity while performing a task. As shown in figure Figure 6.6, it utilizes a structured decision tree to guide individuals through a ten-point rating system, with each level accompanied by a description indicating the corresponding workload intensity [62].

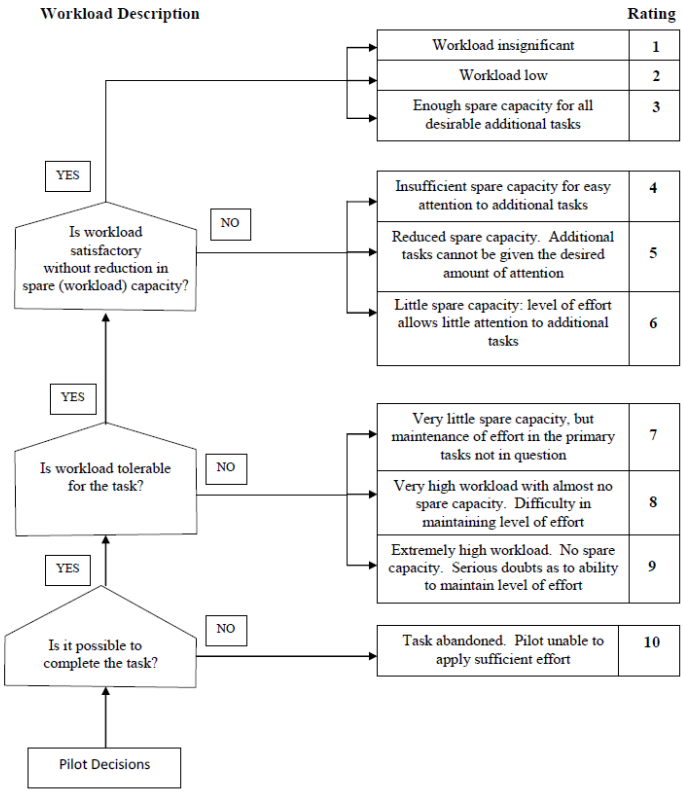

Figure 6.6: Bedford Workload Rating Scale.

Figure Figure 6.7 presents a flowchart illustrating the complete procedure followed during the test execution.

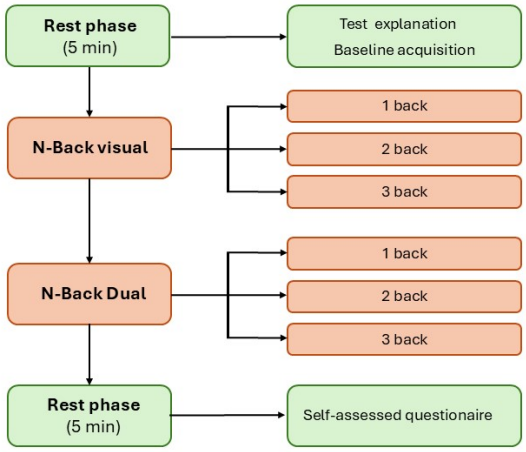

Figure 6.7: Flowchart representing the test procedure adopted for each participant. The different colours highlight the Rest and N-Back phases

Chapter 7

Results

This section presents the obtained results. Initially, the algorithm was evaluated using the Capnobase dataset, focusing solely on respiratory rate analysis. The extracted values were then compared with those reported by the researchers who developed the dataset, using the Smart Fusion algorithm.

After confirming that, the proposed algorithm outperforms the previously introduced approach, it was subsequently tested on an experimental dataset acquired with BiosignalplusX. In this case, in addition to respiratory rate, other features associated with mental workload levels were also assessed. Furthermore, a parallel analysis was conducted on the cardiac component of the signal.

7.1 Capnobase results

The signals in the Capnobase dataset consist of 8-minute recordings. They are segmented into 32-second windows with no overlap, resulting in 15 segments per signal. Before analyzing the extracted PPG signal, the Signal-to-Noise Ratio (SNR) of the reference respiratory signal is computed to prevent inaccurate estimations caused by a corrupted reference. To ensure a conservative estimation, the SNR threshold is set at 20 dB. With 15 analyzable segments per signal, the dataset contains a total of 630 sub-signals. Of these, 251 (40%) were excluded from the analysis due to having an SNR value that was too low. For the remaining 379, the number of "Not a Number" (NaN) occurrences were evaluated and compared with those identified by the Smart Fusion (SF) algorithm. NaN represents cases where the algorithm fails to estimate the respiratory frequency. This comparison allows for an evaluation of the success rates of both methods. The proposed method results in 62 failures out of 379, which accounts for approximately 17% (Figure 7.1) ;the Smart Fusion (SF) algorithm shows 61 NaN occurrences, representing 17% of the total analyzed data too(Figure 7.2).

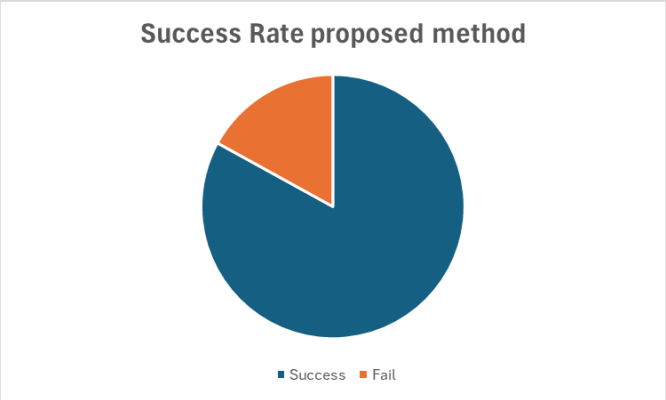

Figure 7.1: Pie chart showing the success rate of the proposed method. In blue the successes, in orange the failures

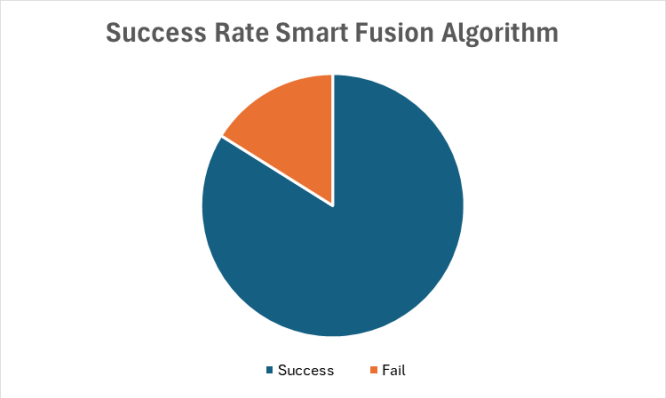

Figure 7.2: Pie chart showing the success rate of the Smart Fusion algorithm. In blue the successes, in orange the failures

Regarding the successful cases, these are directly compared with the reference respiratory rate. This allows for an estimation of the error in terms of breaths per minute.

Below are the graphs illustrating the distribution of the observed errors. Specifically, as shown in Figure 7.3, out of 317 analyzed cases, the respiratory rate was accurately estimated in 270 instances, accounting for approximately 85% of the cases. In 35 occurrences (11% of total cases), the estimation error was 1 breath per minute, while in 5 cases, the respiratory rate was incorrectly assessed with an error of 2 breaths per minute. The remaining errors, along with their respective frequencies, are presented in Table 7.1. As observed, the highest recorded error is 17 breaths per minute, while the average error is 0.32 breaths per minute.

As seen in Figure 7.4, for the Smart Fusion algorithm, although the success rate

Errors(Breaths per minute)	Frequency
0	270
1	35
2	5
3	1
6	2
7	2
9	1
17	1

Table 7.1: Table presenting the errors in terms of breaths per minute observed for the proposed method and their respective frequencies

Figure 7.3: Distribution of error frequency for the proposed algorithm. The histogram illustrates the occurrence of different error values (in breaths per minute), showing a concentration of errors close to zero, with a decreasing frequency for larger errors

remains virtually identical, the distribution of errors varies significantly. Among the 318 analyzed cases, the respiratory rate is accurately estimated in 182 segments, accounting for approximately 57% of the total. An error of one breath per minute occurs 70 times (22% of the total), while an error of two breaths per minute is observed in 20 instances (5%). The remaining errors, along with their respective frequencies, are presented in the following Table 7.2: In this case, the mean error is approximately 1.4214 breaths per minute, while the maximum error reaches 30 breaths per minute.

For the results obtained on the online dataset, a comparison can be made between the outcomes of the proposed method and the 'Smart Fusion' algorithm,

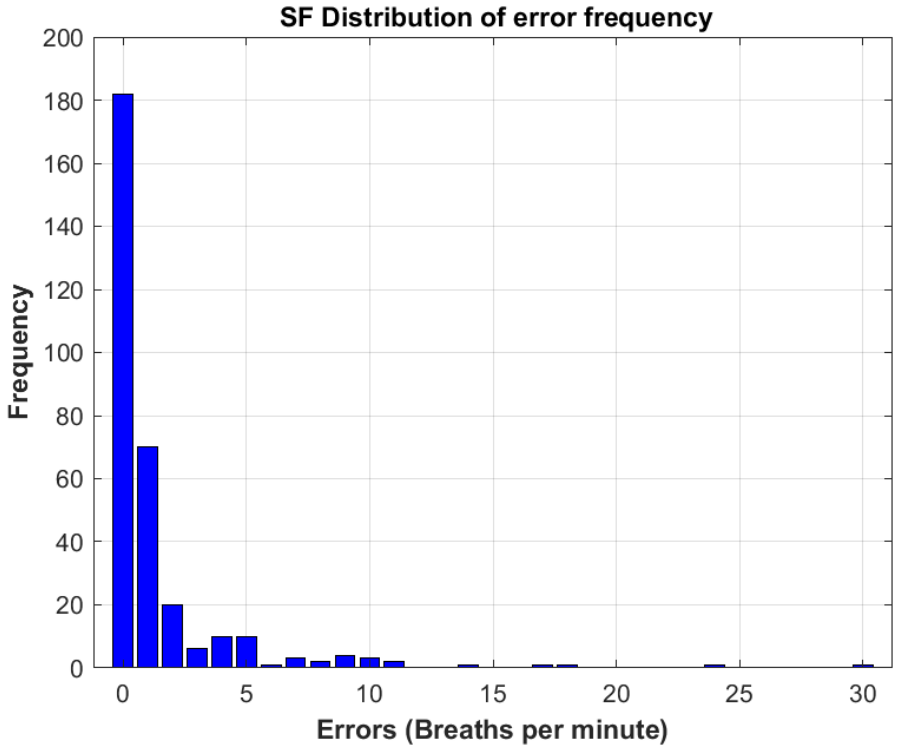

Figure 7.4: Distribution of error frequency for the Smart Fusion (SF) algorithm. The histogram illustrates the occurrence of different error values (in breaths per minute), showing a concentration of errors close to zero, with a decreasing frequency for larger errors

implemented by the same research group that created the database. Although the algorithm is quite conservative, featuring multiple control systems at various scales, the success rate is nearly identical to that achieved using SF. This is attributed to the preprocessing phase, which allows us to work with a cleaner signal, thereby reducing errors. The most notable improvement is in the quality of the errors, as the number and percentage of instances with a '0' error value are significantly higher compared to the reference algorithm. This trend is further supported by the average and maximum error values, which demonstrate a clearly superior performance for the proposed method.

7.2 Experimental data results

The data acquired during the experimental tests were processed using the algorithms described in the previous chapters, both for the cardiac and respiratory components. The signals of eight subjects were analyzed across seven phases: 'rest',

Errors(Breaths per minute)	Frequency
0	182
1	70
2	20
3	6
4	10
5	10
6	1
7	3
8	2
9	4
10	3
11	2
14	1
17	1
18	1
24	1
30	1

Table 7.2: Table presenting the errors in terms of breaths per minute observed for the Smart Fusion Algorithm and their respective frequencies

'1-back visual', '2-back visual', '3-back visual', '1-back dual', '2-back dual', and '3-back dual'. Before processing the results, several tests were conducted using different configurations to determine the most effective approach. The two key parameters adjusted were the observation window length and the overlap. Specifically, experiments were carried out with observation windows of 20, 25, and 30 seconds, where the shorter windows yielded less accurate results. For the overlap, trials with 20, 25, and 28 seconds of overlap were performed. A 25-second overlap was ultimately chosen as the optimal balance between result accuracy and data reliability. A smaller overlap led to poorer performance, while a larger overlap introduced redundancy in the analyzed data.

The test data were processed using 30-second windows with an overlap of approximately 80%, simulating real-time processing. Feature extraction was performed for each window, provided that the signal quality was deemed sufficient. To eliminate inter-subject variability, the data from each participant were subsequently normalized between 0 and 1. This process resulted in the construction of a dataset containing all extracted features associated with the different subjects, along with the mental workload ratings provided by the participants at the end of the test.

After confirming that the variable distributions did not follow a normal distribution, a statistical analysis was conducted to examine the relationship between the normalized variable values and the subjective workload ratings. The Kruskal-Wallis test was selected for this evaluation, as it is a non-parametric test that does not assume normality. The output of this statistical test is the p-value, which, if below 0.05 (considering a 95% confidence level, standard in biomedical research), indicates that the two variables belong to statistically distinct populations. The test was performed on the dataset under both binary classification (rest vs. altered state) and multiclass classification scenarios.

7.2.1 Binary Analysis

The binary analysis was conducted by assigning all data from the 'rest' phase to Class 0, while all data from the altered-state phases ('1-back visual', '2-back visual', '3-back visual', '1-back dual', '2-back dual', and '3-back dual') were assigned to "Class 1". For each cardiac and respiratory feature, the Kruskal-Wallis test was performed, and if the resulting p-value was below 0.05, the feature was considered statistically significant. Table 7.3 presents the number of cardiac and respiratory features that passed the test. It can be observed that 6 out of 19 cardiac features and 4 out of 7 respiratory features exhibited statistically significant differences between the two conditions. The 10 features that met the significance threshold are as follows:

1. Average respiratory rate
2. Average inspiration time
3. Average expiration time
4. Average ventilation
5. Average PPG amplitude
6. Standard deviation of PPG amplitude
7. Median PPG amplitude
8. Standard deviation of PPG duration
9. Median PPG rise time
10. Standard deviation of BPM

	Cardiac(#/19)	**Respiratory (#/7)**
Feature Significance	6	4

Table 7.3: Number of features that passed the Kruskal-Wallis test in the comparison between a resting condition and an altered state.

7.2.2 Multiclass analysis

The analysis across different classes was conducted by comparing all four mental workload conditions: 'rest' (0), 'low' (1), 'medium' (2), and 'high' (3). The Kruskal-Wallis test was initially applied at a global level to determine whether a specific feature exhibited statistically significant differences in at least one of the classes compared to the others. Subsequently, pairwise comparisons were performed, specifically:

1. rest vs low
2. rest vs medium
3. rest vs high
4. low vs medium
5. low vs high
6. medium vs high

Table 7.4 presents the number of features that passed the test across different comparisons. As observed, the number of cardiac and respiratory features exhibiting statistically significant differences decreases as the number of compared classes increases, with only one feature maintaining statistical significance across nearly all comparisons. The most significant features identified are:

1. Average respiratory rate
2. Average inspiration time
3. Average expiration time
4. Average ventilation
5. Average PPG amplitude
6. Median PPG amplitude
7. Standard deviation of PPG duration

8. Standard deviation of BPM

Notably, these features are the same as those that demonstrated statistical significance in the binary analysis, further reinforcing their relevance. The most significant feature identified is the average respiratory rate.

	Cardiac(#/19)	**Respiratory (#/7)**
Feature Significance	13	7
Feature Significance (>1)	12	7
Feature Significance (>2)	7	6
Feature Significance (>3)	4	4
Feature Significance (>4)	0	1
Feature Significance (>5)	0	1

Table 7.4: Number of features that passed the Kruskal-Wallis test in the comparison between all states.

Chapter 8

Conclusions

The goal of this thesis is to investigate whether it is possible to leverage the photoplethysmographic (PPG) signal to simultaneously extract both cardiac and respiratory features in real-time, relative to the acquisition, for monitoring stress levels and mental workload. If successful, the study would enable the use of wearable devices that could replace traditional acquisition systems, providing greater convenience for the operator. Since the relationship between the cardiac component and PPG has been well-explored over the years, this work focused on developing an algorithm for extracting a surrogate respiratory signal, from which the respective features could be derived. The challenge here was not only to extract the respiratory frequency but also to attempt to reconstruct a signal that is morphologically similar to the original one.

Since respiration manifests almost as a low-frequency motion artifact within the PPG signal, an algorithm was developed with multiple verification mechanisms at different scales, prioritizing estimation quality over the sheer number of estimates obtained for the analyzed segments.

The respiratory algorithm was first tested on the publicly available 'Capnobase' dataset to evaluate the estimation quality of respiratory rate against a reference signal. The 8-minute signals are first segmented into 32-second windows without overlap before being processed. The results were compared with those obtained using the Smart Fusion algorithm, which was employed by the same research group that collected the data. The comparison included success rate, error distribution and frequency, mean error, and maximum reported error.

Despite being a highly conservative method, the proposed approach achieved the same success rate as Smart Fusion (17%). However, in terms of error quality, the proposed algorithm demonstrated superior performance, achieving a significantly higher percentage of perfect estimates (80% vs. 57%), a lower mean error (0.31 breaths per minute vs. 1.42 breaths per minute), and a lower maximum error (17 breaths per minute vs. 30 breaths per minute).

The recorded PPG signal was subsequently processed under simulated real-time conditions using 30-second windows with an 80% overlap. For each window meeting the required quality standards, cardiac and respiratory features were extracted. Statistical analyses were then performed to assess the effectiveness of these features in discriminating between different levels of mental workload. Given the non-normal distribution of the extracted features, the Kruskal-Wallis test, a non-parametric statistical method, was applied. If the p-value obtained from this test was below 0.05, it indicated a statistically significant difference between distributions.

The analyses were conducted in two distinct scenarios. In the binary classification, data were categorized into two groups: rest and altered state, leading to the selection of approximately 10 out of 19 analyzed features. In the multiclass classification, all six possible output conditions were compared, and the frequency with which a feature met the statistical significance threshold across comparisons was assessed. The results revealed that the features identified as statistically relevant in the binary case were also those most frequently selected in the multiclass analysis.

The findings from these tests confirm the feasibility of using PPG not only for extracting cardiac features but also for deriving respiratory features. The ability to utilize PPG as an alternative to more specialized physiological signals enhances its applicability across a broader range of scenarios, benefiting from its greater wearability and reduced physical constraints.

Bibliography

[1] G. Fink. «Stress: Concepts, Definition and History». In: *Reference Module in Neuroscience and Biobehavioral Psychology*. Elsevier, Jan. 1, 2017. ISBN: 978-0-12-809324-5. DOI: 10.1016/B978-0-12-809324-5.02208-2. URL: https://www.sciencedirect.com/science/article/pii/B9780128093245022082 (visited on 01/08/2025) (cit. on p. 1).

[2] European Foundation for the Improvement of Living and Working Conditions. and European Agency for Safety and Health at Work. *Psychosocial risks in Europe :prevalence and strategies for prevention : a joint report from the European Foundation for the Improvement of Living and Working Conditions and the European Agency for Safety and Health at Work*. LU: Publications Office, 2014. URL: https://data.europa.eu/doi/10.2806/70971 (visited on 01/19/2025) (cit. on pp. 1, 2).

[3] Razia A.G. Khammissa, Simon Nemutandani, Gal Feller, Johan Lemmer, and Liviu Feller. «Burnout phenomenon: neurophysiological factors, clinical features, and aspects of management». In: *J Int Med Res* 50.9 (Sept. 13, 2022), p. 03000605221106428. ISSN: 0300-0605. DOI: 10.1177/03000605221106428. URL: https://www.ncbi.nlm.nih.gov/pmc/articles/PMC9478693/ (visited on 01/26/2025) (cit. on p. 1).

[4] *Burn-out an occupational phenomenon*. URL: https://www.who.int/standards/classifications/frequently-asked-questions/burn-out-an-occupational-phenomenon (visited on 01/22/2025) (cit. on p. 1).

[5] Fumihiko Yasuma and Jun-Ichiro Hayano. «Respiratory sinus arrhythmia: why does the heartbeat synchronize with respiratory rhythm?» In: *Chest* 125.2 (Feb. 2004), pp. 683–690. ISSN: 0012-3692. DOI: 10.1378/chest.125.2.683 (cit. on p. 2).

[6] Denisse Castaneda, Aibhlin Esparza, Mohammad Ghamari, Cinna Soltanpur, and Homer Nazeran. «A review on wearable photoplethysmography sensors and their potential future applications in health care». In: *Int J Biosens Bioelectron* 4.4 (2018), pp. 195–202. ISSN: 2573-2838. DOI: 10.15406/ijbsbe.

2018.04.00125. URL: https://www.ncbi.nlm.nih.gov/pmc/articles/PMC6426305/ (visited on 01/26/2025) (cit. on p. 2).

[7] Oura Team. *Technology in the Oura Ring*. The Pulse Blog. Feb. 7, 2024. URL: https://ouraring.com/blog/ring-technology/ (visited on 01/26/2025) (cit. on p. 3).

[8] Alessandro Montanari, Andrea Ferlini, Ananta Narayanan Balaji, Cecilia Mascolo, and Fahim Kawsar. «EarSet: A Multi-Modal Dataset for Studying the Impact of Head and Facial Movements on In-Ear PPG Signals». In: *Sci Data* 10.1 (Dec. 1, 2023). Publisher: Nature Publishing Group, p. 850. ISSN: 2052-4463. DOI: 10.1038/s41597-023-02762-3. URL: https://www.nature.com/articles/s41597-023-02762-3 (visited on 01/26/2025) (cit. on p. 3).

[9] *Stress, individui e società | eBook e Libro - Liguori Editore*. URL: http://www.liguori.it/schedanew.asp?isbn=3952 (visited on 01/26/2025) (cit. on p. 5).

[10] Hans Selye. «Stress and the General Adaptation Syndrome». In: *Br Med J* 1.4667 (June 17, 1950), pp. 1383–1392. ISSN: 0007-1447. URL: https://www.ncbi.nlm.nih.gov/pmc/articles/PMC2038162/ (visited on 01/26/2025) (cit. on p. 5).

[11] Cary L. Cooper. «Sources of Stress on Managers at Work». In: *Psychology and Management: A text for managers and trade unionists*. Ed. by Cary L. Cooper. London: Macmillan Education UK, 1981, pp. 201–221. ISBN: 978-1-349-16551-3. DOI: 10.1007/978-1-349-16551-3_10. URL: https://doi.org/10.1007/978-1-349-16551-3_10 (visited on 01/26/2025) (cit. on p. 6).

[12] *Strategic Stress Management: An Organisational Approach20011Valerie J. Sutherland and Cary L. Cooper. Strategic Stress Management: An Organisational Approach . Basingstoke: Macmillan Press 2000. 263 pp. , ISBN: ISBN 0-333-77487-6 £18.99 (paperback) | Request PDF*. URL: https://www.researchgate.net/publication/280189496_Strategic_Stress_Management_An_Organisational_Approach20011Valerie_J_Sutherland_and_Cary_L_Cooper_Strategic_Stress_Management_An_Organisational_Approach_Basingstoke_Macmillan_Press_2000_263_pp_ISBN_IS (visited on 01/26/2025) (cit. on p. 6).

[13] *Stress:modelli teorici - In-Psychology*. URL: https://www.in-psychology.it/stressmodelli-teorici/ (visited on 01/26/2025) (cit. on p. 6).

[14] Luca Mastrogiacomo and Riccardo Gervasi. «Valutazione dello stress mentale e del carico di lavoro cognitivo attraverso i dati di eye-tracking». In: () (cit. on p. 8).

[15] D. W. Jahns. *A Concept of Operator Workload in Manual Vehicle Operations*. Google-Books-ID: aSAuvwEACAAJ. Ges. zur Förderung d. Astrophysikal. Forschung, 1973. 88 pp. (cit. on p. 8).

[16] *Human Mental Workload: A Survey and a Novel Inclusive Definition - PMC*. URL: https://pmc.ncbi.nlm.nih.gov/articles/PMC9201728/ (visited on 01/26/2025) (cit. on p. 8).

[17] Neville Moray. «Models and Measures of Mental Workload». In: Jan. 1, 1979, pp. 13–21. ISBN: 978-1-4757-0886-8. DOI: 10.1007/978-1-4757-0884-4_2 (cit. on p. 9).

[18] Sean Stein Smith. «The Academic Workload». In: *Shifting from Accounting Practitioner to Academia: Tactics, Tips, and Strategies for the Transition*. Ed. by Sean Stein Smith. Cham: Springer International Publishing, 2021, pp. 87–145. ISBN: 978-3-030-67546-2. DOI: 10.1007/978-3-030-67546-2_5. URL: https://doi.org/10.1007/978-3-030-67546-2_5 (visited on 01/26/2025) (cit. on p. 9).

[19] Walter Rohmert. «Determination of Stress and Strain at Real Work Places: Methods and Results of Field Studies with Air Traffic Control Officers». In: *Mental Workload: Its Theory and Measurement*. Ed. by Neville Moray. Boston, MA: Springer US, 1979, pp. 423–443. ISBN: 978-1-4757-0884-4. DOI: 10.1007/978-1-4757-0884-4_26. URL: https://doi.org/10.1007/978-1-4757-0884-4_26 (visited on 01/26/2025) (cit. on p. 10).

[20] *Establishment of overall workload assessment technique for various tasks and workplaces - ScienceDirect*. URL: https://www.sciencedirect.com/science/article/pii/S0169814101000403?casa_token=V22QHiNXk4QAAAAA:72fCSoXt_RE99sXVdbVemz0RuSSf1WxrF0sKXQHk4BqwOVwTXicP557Zi4zX26Yrf-i608qM (visited on 01/26/2025) (cit. on p. 10).

[21] *Burnout - an overview | ScienceDirect Topics*. URL: https://www.sciencedirect.com/topics/medicine-and-dentistry/burnout (visited on 01/26/2025) (cit. on p. 10).

[22] Christina Maslach, Susan Jackson, and Michael Leiter. «The Maslach Burnout Inventory Manual». In: *Evaluating Stress: A Book of Resources*. Vol. 3. Journal Abbreviation: Evaluating Stress: A Book of Resources. Jan. 1, 1997, pp. 191–218 (cit. on p. 10).

[23] *PsycNET Record Display*. URL: https://psycnet.apa.org/record/1986-98619-020 (visited on 01/26/2025) (cit. on p. 13).

[24] Luca Longo, Christopher D. Wickens, Gabriella Hancock, and P. A. Hancock. «Human Mental Workload: A Survey and a Novel Inclusive Definition». In: *Front Psychol* 13 (June 2, 2022), p. 883321. ISSN: 1664-1078. DOI: 10.3389/fpsyg.2022.883321. URL: https://www.ncbi.nlm.nih.gov/pmc/articles/PMC9201728/ (visited on 01/26/2025) (cit. on pp. 14, 18, 19).

[25] Sandra G. Hart and Christopher D. Wickens. «Workload Assessment and Prediction». In: *Manprint: An Approach to Systems Integration*. Ed. by Harold R. Booher. Dordrecht: Springer Netherlands, 1990, pp. 257–296. ISBN: 978-94-009-0437-8. DOI: 10.1007/978-94-009-0437-8_9. URL: https://doi.org/10.1007/978-94-009-0437-8_9 (visited on 01/26/2025) (cit. on p. 15).

[26] Fred Zijlstra. «Efficiency in Work Behavior: A Design Approach for Modern Tools». In: (Jan. 1, 1993) (cit. on p. 15).

[27] A. J. Tattersall and P. S. Foord. «An experimental evaluation of instantaneous self-assessment as a measure of workload». In: *Ergonomics* 39.5 (May 1996), pp. 740–748. ISSN: 0014-0139. DOI: 10.1080/00140139608964495 (cit. on p. 15).

[28] J. G. Casali and W. W. Wierwille. «A comparison of rating scale, secondary-task, physiological, and primary-task workload estimation techniques in a simulated flight task emphasizing communications load». In: *Hum Factors* 25.6 (Dec. 1983), pp. 623–641. ISSN: 0018-7208. DOI: 10.1177/001872088302500602 (cit. on p. 15).

[29] Bruce Roscoe, Mark S. Diana, and Richard H. Brooks. «Early, middle, and late adolescents' views on dating and factors influencing partner selection». In: *Adolescence* 22.85 (1987). Place: US Publisher: Libra Publishers, pp. 59–68. ISSN: 0001-8449 (cit. on p. 15).

[30] *Development of NASA-TLX (Task Load Index): Results of Empirical and Theoretical Research - ScienceDirect*. URL: https://www.sciencedirect.com/science/article/abs/pii/S0166411508623869 (visited on 01/26/2025) (cit. on p. 15).

[31] P. S. Tsang and V. L. Velazquez. «Diagnosticity and multidimensional subjective workload ratings». In: *Ergonomics* 39.3 (Mar. 1996), pp. 358–381. ISSN: 0014-0139. DOI: 10.1080/00140139608964470 (cit. on p. 15).

[32] *The Subjective Workload Assessment Technique: A Scaling Procedure for Measuring Mental Workload - ScienceDirect*. URL: https://www.sciencedirect.com/science/article/abs/pii/S0166411508623870 (visited on 01/26/2025) (cit. on p. 15).

[33] *Reading comprehension difficulties: Correlates, causes, and consequences | Request PDF*. URL: https://www.researchgate.net/publication/310842774_Reading_comprehension_difficulties_Correlates_causes_and_consequences (visited on 01/26/2025) (cit. on p. 15).

[34] Asit Dey and Danny D. Mann. «Sensitivity and diagnosticity of NASA-TLX and simplified SWAT to assess the mental workload associated with operating an agricultural sprayer». In: *Ergonomics* 53.7 (2010). Place: United Kingdom Publisher: Taylor & Francis, pp. 848–857. ISSN: 1366-5847. DOI: 10.1080/00140139.2010.489960 (cit. on p. 15).

[35] Paul Miller and Junko Kozu. «Miller et al 2001 Social influence, empathy, and prosocial behavior in cross-cultural perspective copy». In: (Jan. 1, 2001) (cit. on pp. 18, 19).

[36] Christopher D. Wickens, Robert S. Gutzwiller, and Amy Santamaria. «Discrete task switching in overload: A meta-analyses and a model». In: *International Journal of Human-Computer Studies* 79 (July 2015), pp. 79–84. ISSN: 10715819. DOI: 10.1016/j.ijhcs.2015.01.002. URL: https://linkinghub.elsevier.com/retrieve/pii/S1071581915000051 (visited on 01/26/2025) (cit. on p. 19).

[37] Anne Carswell, Mary Ann McColl, Sue Baptiste, Mary Law, Helene Polatajko, and Nancy Pollock. «The Canadian Occupational Performance Measure: a research and clinical literature review». In: *Can J Occup Ther* 71.4 (Oct. 2004), pp. 210–222. ISSN: 0008-4174. DOI: 10.1177/000841740407100406 (cit. on p. 19).

[38] Gerhard Marquart, Christopher Cabrall, and Joost de Winter. «Review of Eye-related Measures of Drivers' Mental Workload». In: *Procedia Manufacturing* 3 (Dec. 31, 2015). DOI: 10.1016/j.promfg.2015.07.783 (cit. on p. 19).

[39] J. Miller, C. G. Wilson, and D. G. Uttamchandani. «An optoelectronic system for intra-ocular drug detection». In: *Proceedings of SPIE: The International Society for Optical Engineering* 4263.48 (2001). Num Pages: 6 Number: 48, pp. 48–54. URL: https://doi.org/10.1117/12.429346 (visited on 03/06/2025) (cit. on p. 19).

[40] *Acute Aminoglycoside Retinal Toxicity In Vivo and In Vitro | IOVS | ARVO Journals*. URL: https://iovs.arvojournals.org/article.aspx?articleid=2124530 (visited on 03/06/2025) (cit. on p. 20).

[41] J. R. Bassett, P. M. Marshall, and R. Spillane. «The physiological measurement of acute stress (public speaking) in bank employees». In: *International Journal of Psychophysiology* 5.4 (Dec. 1, 1987), pp. 265–273. ISSN: 0167-8760. DOI: 10.1016/0167-8760(87)90058-4. URL: https://www.sciencedirect.

com/science/article/pii/0167876087900584 (visited on 03/06/2025) (cit. on p. 20).

[42] G. Luzzani, I. Buraioli, D. Demarchi, and G. Guglieri. «A review of physiological measures for mental workload assessment in aviation: A state-of-the-art review of mental workload physiological assessment methods in human-machine interaction analysis». In: *Aeronaut. j.* 128.1323 (May 2024), pp. 928–949. ISSN: 0001-9240, 2059-6464. DOI: 10.1017/aer.2023.101. URL: https://www.cambridge.org/core/product/identifier/S000192402300101X/type/journal_article (visited on 01/27/2025) (cit. on p. 20).

[43] Usman Ghani, Nada Signal, Imran Khan Niazi, and Denise Taylor. «ERP based measures of cognitive workload: A review». In: *Neurosci Biobehav Rev* 118 (Nov. 2020), pp. 18–26. ISSN: 1873-7528. DOI: 10.1016/j.neubiorev.2020.07.020 (cit. on p. 20).

[44] Paul Ayres, Joy Yeonjoo Lee, Fred Paas, and Jeroen J. G. van Merriënboer. «The Validity of Physiological Measures to Identify Differences in Intrinsic Cognitive Load». In: *Front Psychol* 12 (2021), p. 702538. ISSN: 1664-1078. DOI: 10.3389/fpsyg.2021.702538 (cit. on p. 20).

[45] Essam Debie, Raul Fernandez Rojas, Justin Fidock, Michael Barlow, Kathryn Kasmarik, Sreenatha Anavatti, Matt Garratt, and Hussein A. Abbass. «Multimodal Fusion for Objective Assessment of Cognitive Workload: A Review». In: *IEEE Trans Cybern* 51.3 (Mar. 2021), pp. 1542–1555. ISSN: 2168-2275. DOI: 10.1109/TCYB.2019.2939399 (cit. on p. 20).

[46] J. Satheesh Kumar and P. Bhuvaneswari. «Analysis of Electroencephalography (EEG) Signals and Its Categorization–A Study». In: *Procedia Engineering* 38 (2012), pp. 2525–2536. ISSN: 18777058. DOI: 10.1016/j.proeng.2012.06.298. URL: https://linkinghub.elsevier.com/retrieve/pii/S1877705812022114 (visited on 01/27/2025) (cit. on p. 20).

[47] Todd Handy. *Event-related potentials: A handbook*. Jan. 1, 2005 (cit. on p. 20).

[48] M. Kalaivani, Senthil Amudhan, Ashish Upadhyay, and Vineet Kamal. «Biostatistics». In: *Essentials of Neuroanesthesia*. Journal Abbreviation: Essentials of Neuroanesthesia. Dec. 31, 2017, pp. 975–995. ISBN: 978-0-12-805299-0. DOI: 10.1016/B978-0-12-805299-0.00063-4 (cit. on p. 21).

[49] *Basic study of visual systems for sea pilot simulator training - Murai - 2008 - IEEJ Transactions on Electrical and Electronic Engineering - Wiley Online Library*. URL: https://onlinelibrary.wiley.com/doi/abs/10.1002/tee.20338 (visited on 01/26/2025) (cit. on p. 21).

[50] Mieko Ohsuga, Futomi Shimono, and Hirokazu Genno. «Assessment of phasic work stress using autonomic indices». In: *International Journal of Psychophysiology*. Psychophysiology in 40.3 (Apr. 1, 2001), pp. 211–220. ISSN: 0167-8760. DOI: 10.1016/S0167-8760(00)00189-6. URL: https://www.sciencedirect.com/science/article/pii/S0167876000001896 (visited on 01/26/2025) (cit. on p. 21).

[51] AURORA TIVERON. «Rilevamento non invasivo di parametri vitali in dispositivi indossabili tramite fotopletismografia: principio di funzionamento e applicazioni». In: (Oct. 17, 2024). Accepted: 2023-03-23T07:22:05Z. URL: https://thesis.unipd.it/handle/20.500.12608/44067 (visited on 01/26/2025) (cit. on p. 21).

[52] K. Nakajima, T. Tamura, and H. Miike. «Monitoring of heart and respiratory rates by photoplethysmography using a digital filtering technique». In: *Medical Engineering & Physics* 18.5 (July 1, 1996), pp. 365–372. ISSN: 1350-4533. DOI: 10.1016/1350-4533(95)00066-6. URL: https://www.sciencedirect.com/science/article/pii/1350453395000666 (visited on 01/23/2025) (cit. on p. 31).

[53] J. Lee and K. H. Chon. «Respiratory rate extraction via an autoregressive model using the optimal parameter search criterion». In: *Ann Biomed Eng* 38.10 (Oct. 2010), pp. 3218–3225. ISSN: 1573-9686. DOI: 10.1007/s10439-010-0080-9 (cit. on p. 32).

[54] Hodam Kim, Jeong-Youn Kim, and Chang-Hwan Im. «Fast and Robust Real-Time Estimation of Respiratory Rate from Photoplethysmography». In: *Sensors (Basel)* 16.9 (Sept. 14, 2016), p. 1494. ISSN: 1424-8220. DOI: 10.3390/s16091494 (cit. on p. 32).

[55] Paul A. Leonard, J. Graham Douglas, Neil R. Grubb, David Clifton, Paul S. Addison, and James N. Watson. «A fully automated algorithm for the determination of respiratory rate from the photoplethysmogram». In: *J Clin Monit Comput* 20.1 (Feb. 2006), pp. 33–36. ISSN: 1387-1307. DOI: 10.1007/s10877-005-9007-7 (cit. on p. 34).

[56] Marco Pogliano. «Contactless human vital signals monitoring based on a FMCW Radar». laurea. Politecnico di Torino, Dec. 14, 2022. 112 pp. URL: https://webthesis.biblio.polito.it/25758/ (visited on 01/24/2025) (cit. on p. 34).

[57] Hervé Abdi and Lynne Williams. «Principal Component Analysis». In: *Wiley Interdisciplinary Reviews: Computational Statistics* 2 (July 1, 2010), pp. 433–459. DOI: 10.1002/wics.101 (cit. on p. 34).

[58] Erika Pittella, Anna Bottiglieri, Stefano Pisa, and Marta Cavagnaro. «Cardiorespiratory Frequency Monitoring Using the Principal Component Analysis Technique on UWB Radar Signal». In: *International Journal of Antennas and Propagation* 2017 (Mar. 2, 2017), pp. 1–6. DOI: 10.1155/2017/4803752 (cit. on p. 35).

[59] *biosignalsplux*. PLUX Biosignals. URL: https://www.pluxbiosignals.com/collections/biosignalsplux (visited on 02/06/2025) (cit. on p. 36).

[60] Walter Karlen, M Turner, Erin Cooke, Guy Dumont, and Mark Ansermino. *CapnoBase: Signal database and tools to collect, share and annotate respiratory signals*. Jan. 1, 2010 (cit. on p. 43).

[61] Mohamed Elgendi. «Optimal Signal Quality Index for Photoplethysmogram Signals». In: *Bioengineering (Basel)* 3.4 (Sept. 22, 2016), p. 21. ISSN: 2306-5354. DOI: 10.3390/bioengineering3040021. URL: https://www.ncbi.nlm.nih.gov/pmc/articles/PMC5597264/ (visited on 03/09/2025) (cit. on p. 49).

[62] Edward Bachelder and Martine Godfroy-Cooper. *Pilot Workload Estimation: Synthesis of Spectral Requirements Analysis and Weber's Law*. Jan. 7, 2019. DOI: 10.2514/6.2019-1228 (cit. on p. 60).